Scholars' Mine

Doctoral Dissertations   Student Theses and Dissertations

Summer 2019

Underwater acoustic communications and adaptive signal processing

Mohammadhossein Behgam

Follow this and additional works at: https://scholarsmine.mst.edu/doctoral_dissertations

Part of the Electrical and Computer Engineering Commons

Department: Electrical and Computer Engineering

Recommended Citation

UNDERWATER ACOUSTIC COMMUNICATIONS AND ADAPTIVE SIGNAL

PROCESSING

by

MOHAMMADHOSSEIN BEHGAM

A DISSERTATION

Presented to the Graduate Faculty of the

MISSOURI UNIVERSITY OF SCIENCE AND TECHNOLOGY

In Partial Fulfillment of the Requirements for the Degree

DOCTOR OF PHILOSOPHY

in

ELECTRICAL ENGINEERING

2019

Approved by

Daryl Beetner, Advisor
Yahong Rosa Zheng, Co-Advisor
Kurt Kosbar
Randy Moss
David Pommerenke
Eugene Insall Jr

PUBLICATION DISSERTATION OPTION

This dissertation consists of the following two articles which have been submitted for publication as follows:

Paper I: (Pages 5-35) M. Behgam, Y. R. Zheng, Z. Liu, "Tail-Biting Convolutional Codes for Underwater Acoustic Communications with Short Packets" has been submitted to IEEE J. Ocean. Eng, Feb 2019.

Paper II: (Pages 36-55) M. Behgam, X. Qin, Y. R. Zheng, "Passband Data Reuse of Field Experimental Data in Underwater Acoustic Communications" is intended for submission to IEEE J. Ocean. Eng.

ABSTRACT

This dissertation proposes three new algorithms for underwater acoustic wireless communications. One is a new tail-biting circular MAP decoder for full tail-biting convolution (FTBC) codes for very short data blocks intended for Internet of Underwater Things (IoUT). The proposed algorithm was evaluated by ocean experiments and computer simulations on both Physical (PHY) and Media access control (MAC) layers. The ocean experimental results show that without channel equalization, the full tail-biting convolution (FTBC) codes with short packet lengths not only can perform similarly to zero-tailing convolution (ZTC) codes in terms of bit error rate (BER) in the PHY layer. Computer simulation results show that the FTBC codes outperform the ZTC codes in terms of MAC layer metrics, such as collision rate and bandwidth utilization, in a massive network of battery powered IoUT devices.

Second, this dissertation also proposes a new approach to utilizing the underwater acoustic (UWA) wireless communication signals acquired in a real-world experiment as a tool for evaluating new coding and modulation schemes in realistic doubly spread UWA channels. This new approach, called passband data reuse, provides detailed procedures for testing the signals under test (SUT) that change or add error correction coding, change bit to symbol mapping (baseband modulation) schemes from a set of original experimental data.

ACKNOWLEDGMENTS

First and foremost, I would like to acknowledge my advisor Dr. Yahong Rosa Zheng. I sincerely appreciate her continuous support and devoted guidance throughout my Ph.D study. Without her numerous constructive suggestions, insightful comments and generous financial support, this dissertation would have been impossible. Her enthusiasm, dedication and down-to-earth attitude towards research have set a role model of academic perfection, from which I will benefit in my future career.

This dissertation, in particular, is dedicated to the memory of Dr. Steven L. Grant, who was my advisor from 2014 to 2016 until he pass away in April 2016.

I would like to express my sincere thanks to the ECE department chair, Dr. Daryl Beetner, for his permission to use the Wilkins Missouri Telecommunications endowment fund to support me through the last year of my Ph.D. study.

I also would like to thank the members of my Ph.D. advisory committee, Dr.s Kosbar, Moss, Pommerenke, and Insall for their patience and time and valuable advice during my study.

I would like to express my eternal gratitude to my parents and my sister for their unconditional love and support throughout the years.

Finally, I would also like to acknowledge my friends, lab mates in Rolla, MO and Bethlehem, PA for their company, encouragement, and intellectual exchange.

TABLE OF CONTENTS

LIST OF ILLUSTRATIONS

LIST OF TABLES

SECTION

1. INTRODUCTION

1.1. BACKGROUND

Underwater acoustic communications have played a crucial part in the broad range of oceanic engineering applications, such as environmental monitoring, offshore exploration, and disaster prevention. Acoustic waves are not the only means for wireless communication underwater, but they are the only ones that can travel over longer distances. However, current underwater acoustic (UWA) communication systems can only achieve very low data rates such as 1 kbps to 10 kbps at medium range (1 km to 10 km) due to the limited channel bandwidth.

Underwater acoustic channels are amongst the most difficult communication media. Long range acoustic wave propagation is best achieved at low frequencies, and the available bandwidth for communication is extremely limited. Due to the low traveling speed of sound waves, approximately 1500 m/s, and multipath propagation of waves in water, the delay between arrival of each path spreads over tens or even hundreds of milliseconds resulting in frequency-selective signal distortion, which combined with extreme doppler effect caused by ocean currents raise difficult challenges. These properties of acoustic channels degrade the physical link quality and cause high latency in underwater acoustic communications.

Many emerging underwater applications such as autonomous, or unmanned underwater vehicles (AUVs, UUVs) could benefit from real-time wireless communications. Underwater vehicles can move freely without a tether cable and improve their range of operation and while staying connected to an underwater data network consisting of both stationary and mobile nodes (Heidemann *et al.*, 2012) capable of exchanging different types

of data, such as control, telemetry and eventually video signals, between many network nodes. Such a reliable network requires strong error correction coding and channel equalization in the physical layer in order to combat severe impairments from the underwater wireless channels.

Most wireless communication needs are met by exchanging short packets or short data blocks (Durisi *et al.*, 2016). These messages are normally a few bytes in length which aims to keep underwater acoustic sensor nodes (UWASN), instruments connected to the network. These packets are often transmitted sporadically and due to the low propagation speed of sound waves, can cause a massive network of UWASN to suffer from high packet collision rates which reduces the overall throughput of network. Therefore any methods that can effectively increase the network throughput by reducing the packet collision rate are critical to improving the performance of the underwater acoustic networks (UWA-Nets).

1.2. PROBLEM STATEMENT

The bandwidth available in UWA communications is extremely small. Error correction coding techniques and channel equalizations currently used in order to combat the multipath delay spread and Doppler-induced frequency spread that lead to time-varying channel impulse response, reduce the channel bandwidth efficiency. Zero-tailing convolutional forward error correction (FEC) coding schemes increase the number of transmitted bits by adding zeros to the end of the packet in order to make the design of the decoder in the receiver simpler, which causes this technique to suffer from code rate loss, while the channel equalization schemes require long training sequences to estimate the multipath channel impulse response or train the equalizer coefficients. The bandwidth inefficiency becomes significant when a crowded network of UWASN uses short length packets more often to keep the network operating. Thereby, methods that can effectively utilize the limited channel bandwidth are critical to improving the performance of the UWA-Nets.

Second, underwater acoustic (UWA) communications channels lack explicit models that could capture the underlying physics of ocean telemetry and characterize the time-varying doubly-spread nature of channels (Kilfoyle and Baggeroer, 2000). Therefore, many researchers in the field of UWA communications still require sea-going measurement campaigns to evaluate their transmitter and receiver algorithms (van Walree *et al.*, 2008). Holding these campaigns to acquire field data is often expensive, time consuming, and prone to many types of failures (Deane *et al.*, 2018). To reduce the cost of extensive field experiments, researchers in the field of UWA communications have proposed many models and simulators for acoustic communication channels in the past decades. Often the proposed models include a few assumptions, approximations, and simplifications over key parameters of acoustic waves propagation in the ocean (Bjerrum-Niese and Lutzen, 2000; Kilfoyle and Baggeroer, 2000). These parameter include, but are not limited to, wide or quasi-wide sense stationarity, sound speed profiles, sea floor compositions and roughness, time-delay, frequency dispersion, noise or multipath characteristics, etc. These assumptions, although applicable to a specific case or scenario, often lack the knowledge for prediction and evaluation of true long-term ocean channel models.

Motivated by the respective advantages and limitations of the methods in the literature, we proposed a low-complexity receiver algorithms and a novel channel simulator to enable robust UWA communications.

1.3. SUMMARY OF CONTRIBUTION

This dissertation consists of two journal publication papers listed in the publication list. My contributions that are under review are

1. This dissertation proposes an efficient, low computational complexity maximum *A Posteriori* (MAP) decoder designed for full tail-biting convolutional (FTBC) codes for transmitting short data packets in underwater acoustic communications and net-

works. Moreover, the dissertation investigates how much the packet collision rate would improve in underwater acoustic networks that use short messages in communication between nodes, by utilizing FTBC codes as an encoding mechanism to combat underwater channel impairments. The simulation and experimental results on the physical-layer performance demonstrate that the FTBC codes achieve a similar bit error rate (BER) as the conventional method of zero-tailing convolutional (ZTC) codes when applied to different short message lengths, while reducing packet collision rate in an underwater acoustic network.

2. A new type of underwater acoustic channel simulator is proposed based on reusing the passband signal acquired from previous real-world sea trial experiments. This dissertation provides detailed procedures of the passband data reuse method on how a signal under test from previous experiments can be reconfigured in order to be used as a channel simulator. This method enables the possibility of changing or adding new error correction codes or changing the bit to symbol mapping (baseband modulation) schemes of the recorded signal in order to evaluate new coding and modulation schemes in a real-world scenarios.

PAPER

I. TAIL-BITING CONVOLUTIONAL CODES FOR UNDERWATER ACOUSTIC COMMUNICATIONS WITH SHORT PACKETS

Mohammadhossein Behgam, Yahong Rosa Zheng, *Fellow, IEEE*,

Zhiqiang Liu, *Senior Member, IEEE*

ABSTRACT

This paper investigates full tail-biting convolutional (FTBC) codes for transmitting short data packets in underwater acoustic communications and networks. With a constraint length of K and coding rate of $R = 1/n$, the traditional zero-tailing convolutional (ZTC) codes suffer from considerable rate loss when the message length is small, while the FTC codes offer good error correction performance at no coding rate loss. A new circular Maximum *A Posteriori* Probability (MAP) decoding algorithm is proposed to decode the FTBC codes without increasing the computational complexity, when compared to decoding ZTC codes with the MAP algorithm. The new circular MAP decoding algorithm is evaluated by both simulation and a real-world ocean experiment in comparison to the ZTC codes. When applied to networks designed for handling short packet type of traffics, simulation results show that the FTBC codes reduce the network collision rate and improve the network throughput in comparison to the traditional ZTC codes. The simulation results on the physical-layer performance demonstrate that the FTBC codes achieve a similar bit error rate (BER) as the ZTC when applied to different short message lengths. In addition, the ocean experimental results show that the FTBC and ZTC codes achieve acceptable BER on the

order of 1% when the block length is shorter than 64; however when the block length is 64 and larger, all types of codes suffered more from the inter-symbol interference (ISI) induced by the multipath fading channels when no channel equalizer is used.

Keywords: Slotted Aloha, Tail-biting convolutional codes, underwater acoustic communications, Maximum A Posteriori decoding, circular Viterbi algorithm, Internet of Things, Internet of Underwater Things.

1. INTRODUCTION

Underwater acoustic wireless networks (UWA-Nets) are gaining more interest in a variety of applications such as deep ocean exploration, remote underwater command and control, and underwater infrastructure monitoring. These underwater networks, unlike terrestrial radio frequency (RF) wireless networks, face more severe constraints, such as large propagation delay, severe multipath and Doppler, and limited bandwidth. Many protocols such as Aloha and slotted-Aloha are developed for RF networks to provide random channel access. When these protocols are utilized for UWA-Nets, they become more vulnerable to packet collision and channel impairments. The network efficiency also suffers from the large inter-nodal propagation delay in UWA-Nets with respect to the packet length and nodal coverage range.

In the PHY layer, strong error correction coding and channel equalization are often used to combat severe impairments from the underwater wireless channels. The multipath delay spread and Doppler-induced frequency spread lead to time-varying channel impulse responses that cause severe inter-symbol interference and burst bit errors. Channel impairments in underwater acoustic (UWA) communications are more severe than terrestrial RF communications, in that both multipath delay spread and Doppler spread are extremely high. These factors call for extra strong forward error correction (FEC) coding schemes (Chitre *et al.*, 2008; Stojanovic and Preisig, 2009) and complex channel equalization techniques (Stojanovic and Preisig, 2009; Zheng *et al.*, 2015) to improve the reliability of UWA

communication. However, both FEC coding and channel equalization techniques reduce the channel bandwidth efficiency because FEC coding schemes increase the number of transmitted bits, while the channel equalization schemes require long training sequences to estimate the multipath channel impulse response or train the equalizer coefficients.

Unfortunately, the available bandwidth in UWA is very small, which is on the order of kilo-Hertz. Any methods that can effectively utilize the limited channel bandwidth are critical to improving the performance of the UWA-Nets. On the other hand, most wireless communication needs are met by exchanging short packets or short data blocks (Durisi *et al.*, 2016). For example, handshaking in wireless network protocols involves exchange of the Request to Send (RTS) and Clear to Send (CTS) messages between the transmitter and the intended receivers. These messages are often as short as 16 - 32 bits. The recent development in massive machine-to-machine (M2M) communications or Internet of Things (IoT) will support thousands of sensors and smart devices that only transmit short packets sporadically (Boccardi *et al.*, 2014). These messages are normally a few bytes in length. Internet of Underwater Things (Domingo, 2012) also attracts great attention in recent years, which aims to connect underwater sensors, instruments, robots, gliders, and autonomous underwater vehicles (AUVs) to the Internet via underwater wireless links. These underwater devices mostly need short command and control or sensing messages in order to stay connected and communicate with each other.

Therefore, it is often desirable to use a strong FEC coding scheme for short message blocks without complicated channel estimation and equalization for network layer communications. An excellent example is the NATO standard JANUS protocol (Potter *et al.*, 2014), which specifies the network header in a 64-bit message block and codes the block by a constraint length-9 zero-tailed convolutional (ZTC) code, yielding a 144-bit coded block. Using unnecessary long packets for transmission of short data blocks also results in waste of bandwidth resources and increase of latency.

Although the classical iteratively-decodable codes are developed for long packets, code design for short data blocks is gaining traction in recent years (Boccardi *et al.*, 2014; Liva *et al.*, 2016). Conventional FEC codes tend to suffer from coding rate loss and performance loss when applied directly to short data blocks. A recent survey (Liva *et al.*, 2016) on low-density parity check (LDPC) codes, turbo codes, Bose–Chaudhuri–Hocquenghem (BCH) codes, polar codes, and convolutional codes reveals that the LDPC codes exhibit advantages mostly for long data blocks with lengths on the order of several thousand bits or more. In contrast, convolutional codes are known to perform well for short data blocks with lengths on the order of several hundred bits (Clark Jr and Cain, 2013; Lin and Costello, 2004). Convolutional codes are described by (n, k, m) where the code rate is $R = k/n$ and the memory order is $m = K - 1$. The higher the constraint length K or the lower the coding rate, usually the better error correction capability of the code is. Let the data block length be L. For short data blocks with $L < 100$ bits, convolutional codes with a large constraint length would suffer from rate loss because the convolutional codes require m extra zero bits added to the end of the data block to provide equal bit protection all over the information bits, hence the name Zero Tailed Convolutional (ZTC) code, which translates to an effective coding rate of $kL/((L + m)n)$ instead of k/n. When L and K are on the same order, the rate loss is significant. To solve the code rate loss, tail-biting (TB) technique is used to initialize the encoder with the m tail bits (Ma and Wolf, 1986), resulting in the Full Tail-Biting Convolutional (FTBC) codes. FTBC codes retain the coding rate of k/n at the expenses of high decoding complexity if optimal performance is required.

Optimal decoding of FTBC codes is rather complex. Since it is using the last m bits of the data block to initialize the encoder memory prior to encoding the data block and discards the $2m$ output bits corresponding to the initialization, the start state of the code is unknown *a priori* to the decoder. However, the tail-biting technique constrains the start and end states of the encoder to be identical, which requires the decoder to search all possible start states to achieve maximum likelihood (ML) decoding. For codes with a large constraint

length, the complexity becomes prohibitive since it requires 2^m runs of Viterbi decoding. Maximum *A Posteriori* (MAP) decoding of FTBC codes is also available achieving superior performance with more computational complexity (Anderson and Hladik, 1998). Many low-complexity suboptimal algorithms are available in the literature (Anderson and Hladik, 1998, 2002; Cox and Sundberg, 1994; Han *et al.*, 2018; Raghavan and Baum, 1998; Shao *et al.*, 2003; Wang and Bhargava, 1989; Williamson *et al.*, 2014), including the circular Viterbi algorithm (CVA) (Cox and Sundberg, 1994), the Wrap-Around Viterbi Algorithm (WAVA) and Bi-directional VA (BVA) (Shao *et al.*, 2003), the bounded-distance decoding (BDD) CVA(Anderson and Hladik, 2002), the reliability-output Viterbi algorithm (ROVA) (Raghavan and Baum, 1998; Williamson *et al.*, 2014), and two-phase algorithms that acquire trellis metrics in a forward and backward manner in search of the ML path (Han *et al.*, 2018). These algorithms are iterative in nature and have less complexity than the brute force ML algorithm.

Although the maximum-likelihood Viterbi algorithm tries to minimize the probability of code word error for convolutional codes, it does not necessarily minimize the symbol error (Bahl *et al.*, 1974). This problem was tackled by Bahl *et. al.* (Bahl *et al.*, 1974) by estimating and maximizing the *a posteriori* (MAP) probabilities of the states and transitions of a Markov source observed through a noisy discrete memoryless channel to optimally decode the received code word. However, this algorithm is unattractive compared to the Viterbi algorithm from the computational complexity point of view.

This paper applies the FTBC codes to short data blocks for underwater acoustic communications and evaluates their performance by both computer simulation and real-world ocean experiment. This paper improves the tailbiting BCJR algorithm (Anderson and Hladik, 1998) and proposes a new implementation of tailbiting circular MAP (TC-MAP) decoder that achieves much lower computational complexity than that in the tail-baiting BCJR (Anderson and Hladik, 1998). Performance at both MAC-layer and PHY-layer is evaluated for data block lengths from $L = 12, 25, 32, 64$ to $L = 512$. On the MAC-layer, we

simulated an any-to-any network with the slotted-Aloha protocol where a randomly-selected transmission node may communicate with a random receive node at each time slot. The slot length may be shorter than the sum of the propagation delay and the message length. Different coverage areas have been simulated and the maximum propagation delay increases as the area increases. With shorter transmission length, the network collision rate is always lower than that of the longer transmission length. The throughput of shorter transmission length is also higher than the longer transmission length.

On the PHY-layer, computer simulations compared the $K = 3, 6, 9$ rate 1/2 codes in Additive White Gaussian Noise (AWGN) channels and the results show that the FTBC codes with CVA performed similarly with the ZTC codes. The ocean experiment evaluated the (3,1,5) code and (2,1,8) code in real-world UWA fading channels. Results of the ocean experiment show that the (3,1,5) code outperformed the (2,1,8) code due to higher redundancy, and FTB codes performed close to ZTC codes with TC-MAP decoding algorithms. The ocean experiment results also show that the shortest block length $L = 12$ for $K = 6$ and $K = 9$ FTBC codes performed worse than the corresponding ZTC codes because the coded block size was too small to realize the coding gain. The same reason was responsible for the worse performance of the (2,1,8) FTBC codes than those of ZTC codes for $L = 25$ and $L = 32$. The longer block lengths $L = 64$ and $L = 512$ all suffered severe inter-symbol interference (ISI) due to multipath. Without channel equalization, the coding schemes were ineffective in combating the ISI. Therefore, we conclude that the ZTC and FTBC codes with strong error correction capability may be utilized without channel equalization for short data blocks in UWA channels, which enjoy both low computational complexity and high error correction gains (Behgam *et al.*, 2018).

2. FULL TAIL-BITING CONVOLUTIONAL CODES

A typical convolutional encoder is shown in Figure 1,where $K = 3$ rate 1/2 code has $m = K - 1$ memory units $M0$ and $M1$. The code generator is $G = [7, 5]$ in the octal format which corresponds to the generator polynomials $g_1(x) = x^2 + x + 1$ and $g_2(x) = x^2 + 1$. The encoder takes a input bit into the shift register and outputs two bits $c1$ and $c2$. The input bit is shifted to $M0$ when the next input bit arrives.
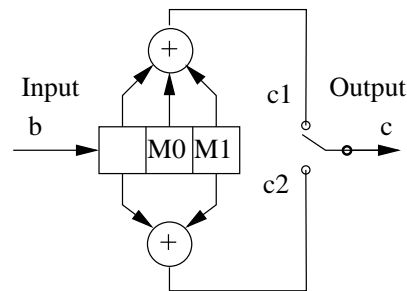
Figure 1. Encoder structure of $K = 3$ rate 1/2 convolutional codes.

2.1. ENCODING TECHNIQUES

A ZTC encoder adds m zeros at the end of the data block to flush out the memory so the ending state is forced back to the all-zero state. This overhead is necessary for reliable transmission because it protects the last m bits in the block. Therefore, total length of the output code word is $n(L + m)$ bits, rather than nL for an $(n, 1, m)$ code resulting in some rate loss. A FTBC code attempts to solve the problem of code rate loss while maintaining equal amount of protection for every bit in the block. The FTBC technique, shown in Figure 2, uses the last m bits of the data block to initialize the encoder memory prior to encoding of the data block, and discards any output from encoder in the initialization stage. In the second stage, the data block is passed through the initialized encoder, and the output codeword is then transmitted. With this technique, total length of the output code word is nL bits. What makes the FTBC technique more complex is that, any valid state of the encoder is equally probable to be the starting and ending states of the encoder. However,

this technique ensures that the encoder starts and ends in an identical state for each data block. This is illustrated in the Trellis diagram in Figure 2 for the $K = 3$, $R = 1/2$ FTBC code. This unique feature is utilized in the decoder to achieve error correction decoding with some increase in decoding complexity over the ZTC decoder.
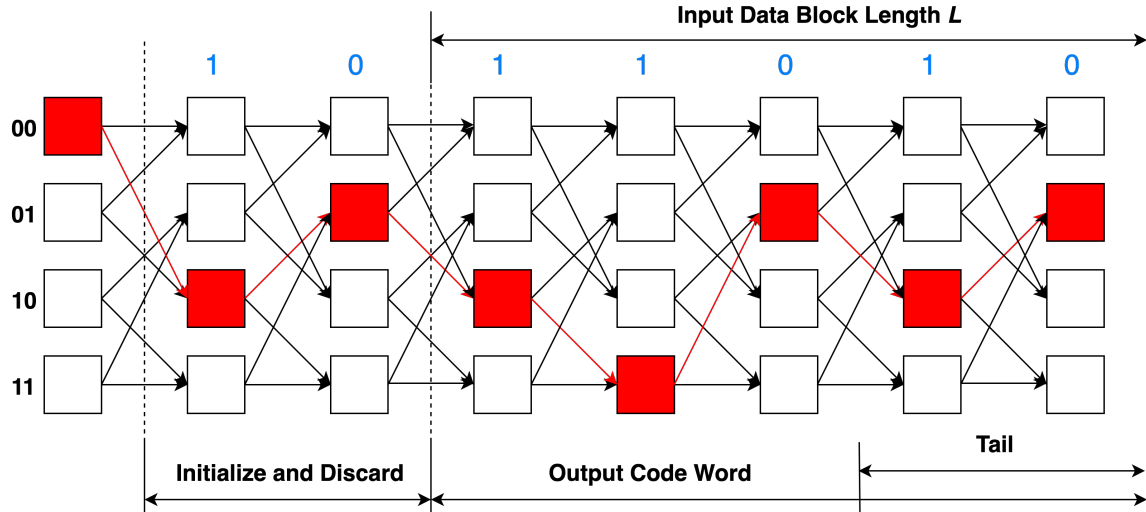
Figure 2. Encoder trellis diagram for tail-biting codes with $K = 3$ and rate 1/2.

2.2. DECODING TECHNIQUES

The Viterbi algorithm (VA) (Viterbi, 1967) is the Maximal Likelihood (ML) decoder for convolutional codes. When applied to the ZTC codes, the branch metric is calculated for each state at each stage of the Trellis diagram. For hard-decision VA, the branch metric is the hamming distance between the received code and the legitimate code, and for soft-decision VA, it is the Euclidean distance between the two. At each stage, the path with the shortest distance entering each state is kept and other branches are discarded. After $3K - 5K$ stages, the survival paths converge to a single path corresponding to the decoded bit sequence. The ending state of the ZTC decoder is also the all-zero state.

However, the situation is different when the VA is applied to FTBC codes. The algorithm must find the best path with the constraint that the maximum likelihood path starts and ends in an identical state which can be any one of the 2^m possible states. It simply

appears that a brute force method to decode a FTBC code is to run VA once for each possible starting state and, then after constructing the path metrics, check if the ending state with the minimum path metric is identical to the starting state. The VA can start decoding from state zero and work its way up to the last state in an orderly fashion, or take a probabilistic approach (Ma and Wolf, 1986) by choosing an arbitrary starting state.

A low-complexity sub-optimal algorithm for FTBC decoding is known as the circular Viterbi algorithm (CVA), where VA traverses around the tail-biting circle more than once (Anderson and Hladik, 2002; Cox and Sundberg, 1994; Shao *et al.*, 2003). In this paper, a CVA with a fixed stopping rule was used to decode FTBC, similar to the lowest-complexity case in (Cox and Sundberg, 1994). The received data block is repeated twice, as shown in Figure 3. The decoder starts with all states having the same starting metric value, constructs the Trellis by calculating the branch metric. At the block boundary, the VA continues passing the received data block three times. The first time is to find the correct start state for the trellis construction for the second copy of the received block; the second time is to construct the output trellis, and the last time is to perform the correct training so that the traceback begins from the correct state. The decoded bit sequence corresponds to the output in the second copy of the received data block.
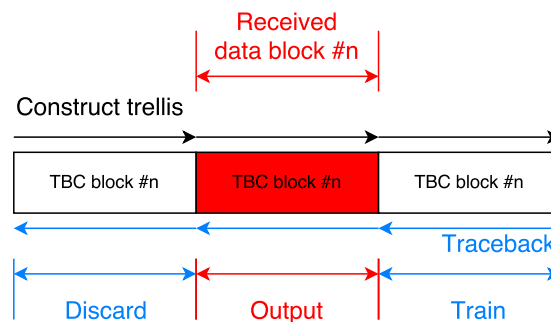
Figure 3. Low-complexity CVA for FTB decoding. The fixed stopping rule is to use three copies of the received data block and traverses the trellis through them.

The CVA applies continuous decoding process to the sequence of appended received data blocks, without losing any (soft) information gathered from decoding the previous copy of the received block, and all the information is transfered to the next attempt to decode the second copy, and so on. The continuous fashion of decoding on a repeated versions of the same received block inherently satisfies the constraint that the FTBC codes have identical start and ending states. Also, the advantage of using short length data blocks is that the traceback length can be equal to data block length ensuring no degradation on the BER performance. One disadvantage of choosing the fixed stopping rule for the CVA is the BER degradation for noisy channels or an increased workload for good channels (Cox and Sundberg, 1994).

3. THE PROPOSED TAILBITING CIRCULAR MAP (TC-MAP) DECODING ALGORITHM

The goal of the MAP decoder is to compute and maximize the *a posteriori* probabilities (APP) that a state i is sent at stage t, given that $\mathbf{y} = y_1, \cdots, y_L$ are the received symbols. Equivalently, the MAP decoder maximizes the joint distribution $p(S_t = s, S_{t+1} = s', \mathbf{y})$, where $S_t = s$ denotes the event that the encoder is in state i at trellis stage t. This joint distribution can be decomposed, using the Bayes' rule, into three parts:

$$p(S_t, S_{t+1}, \mathbf{y}) = p(S_t, [y_1 : y_{t-1}]) \cdot p(S_{t+1}, y_t|S_t) \cdot p([y_{t+1} : y_L]|S_{t+1})$$

$$= \alpha_t(S_t) \cdot \gamma_t(S_t, S_{t+1}) \cdot \beta_{t+1}(S_{t+1}) \tag{1}$$

where α_t, and β_{t+1} are the forward and backward transition metrics, respectively, and γ_t is the branch metric. The three metrics are calculated recursively by

$$\alpha_t(S_t = s) = p(S_t, [y_1 : y_{t-1}]) = \sum_{\forall s' \in \mathcal{S}} \alpha_{t-1}(s') \cdot \gamma_{t-1}(s', s) \tag{2}$$

$$\beta_t(S_t = s) = p([y_t : y_L]|S_t) = \sum_{\forall s' \in \mathcal{S}} \beta_{t+1}(s') \cdot \gamma_t(s, s') \tag{3}$$

$$\gamma_t(S_t = s, S_{t+1} = s') = p(S_{t+1}, y_t|S_t) = P(S_{t+1}|S_t) \cdot p(y_t|S_t, S_{t+1})$$

$$= \begin{cases} p(b_t) \cdot p(y_t|u_t), & \text{valid branch} \\ 0, & \text{invalid branch} \end{cases} \tag{4}$$

where $\mathcal{S}$ is the set of valid states, $p(b_t)$ is the probability of the input bit, being 0 or 1, corresponding to the valid branch of state transition $s \rightarrow s'$, and u_t is the transmitted symbols corresponding to the same state transition. The distribution $p(y_t|u_t)$ is assumed to be Gaussian.

For the ZTC codes, the encoder starts at state zero, so the MAP decoder initializes the alpha and beta metrics as $\boldsymbol{\alpha}_1 = [1, 0, ..., 0]_{1 \times M}$, $\boldsymbol{\beta}_{L+K-1} = [1, 0, ..., 0]_{M \times 1}^T$. The forward-backward algorithm computes the alpha metric from $t = 1$ to $t = L + K$, and the beta metric from $t = L + K - 1$ to $t = 1$. meanwhile, the MAP algorithm computes the gamma metric for all t. The ultimate goal is to compute the *a posteriori* probability $p(\hat{b}_t|\mathbf{y})$. If $p(b_t = 0|y_t) > p(b_t = 1|y_t)$, then the $\hat{b}_t$ is decoded as zero, otherwise, a one. This is equivalent to computing the log likelihood ratio, $LLR(\hat{b}_t|\mathbf{y}) = \ln \frac{p(b_t=1|\mathbf{y})}{p(b_t=0|\mathbf{y})}$. A hard decision can be made based on the LLR output to decode $\hat{b}_t$. That is, $\hat{b}_t = 0$ if $L(\hat{b}_t|\mathbf{y}) < 0$, and $\hat{b}_t = 1$ if $L(\hat{b}_t|\mathbf{y}) > 0$.

Since the FTBC encoder may start at any state in the trellis, the $\boldsymbol{\alpha}_1$ and $\boldsymbol{\beta}_L$ have to be initialized with different approach. Therefore, we propose a novel circular MAP algorithm that initializes the alpha and beta metrics $\boldsymbol{\alpha}_1$ and $\boldsymbol{\beta}_L$ such that all states are equally probable to be the starting and ending state of the encoder. Note that the length of the trellis is only L for the FTBC codes instead of $L + K - 1$ for the ZTC codes. If the same forward-backward algorithm of the ZTC MAP decoder is used for the FTBC codes with a length L trellis, then the $K - 1$ stages would suffer from computational errors. We propose to wrap around the

trellis in the circular fashion with a depth set to be $K - 1$, as shown in Figure 4, where the stage index t progresses in a circular fashion in the range of $[1, L]$ for the alpha and beta metrics.

α_1	α_2	...	α_{L-1}	α_L	α_1	α_2	...	α_{K-2}	α_{K-1}
Initialize	Compute α_t and β_t				Wrap around and update the first $(K-1)_{\text{stages}}$				
β_L	β_{L-1}	...	β_2	β_1	β_L	β_{L-1}	...	$\beta_{L-(K-1)+2}$	$\beta_{L-(K-1)+1}$

t
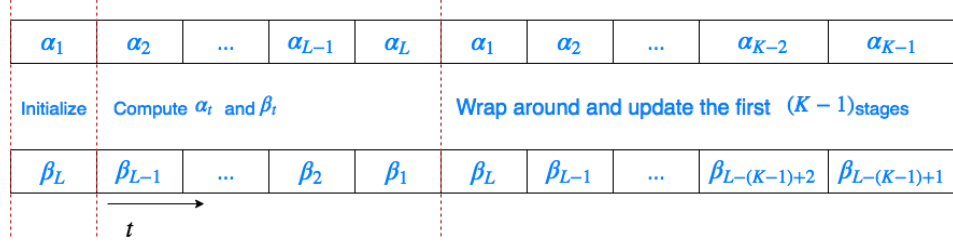
Figure 4. TC-MAP decoding algorithm stage indexing order.

The proposed wrap-around depth is much smaller than the ones in the tailbiting BCJR (Anderson and Hladik, 1998) which uses a stopping criterion measured by $\Delta = ||\alpha_t - \alpha_t'||$, i.e. the algorithm stops if the change in newly computed α_t array is suitably small to the previously computed one α_t' at index t. We discover that this measure demonstrates a significant drop of value at stage $K - 1$ beyond L, even for low SNRs, as shown in Figure 5. Therefore, we propose the new implementation to stop at stage $K - 1$ beyond L without calculating the stopping criterion. This simplification ensures that the proposed TC-MAP algorithm is robust against noise estimation errors and is independent from threshold settings or SNR estimates.
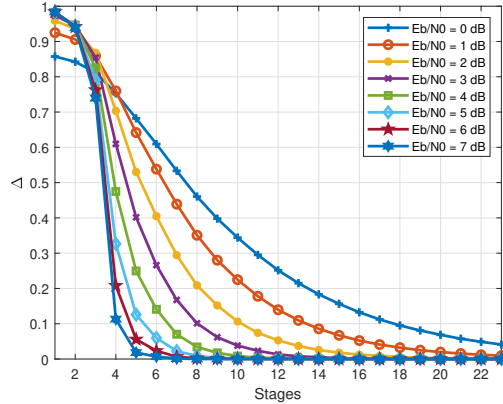
Figure 5. Stopping criteria used in (Anderson and Hladik, 1998): $\Delta = ||\alpha_t - \alpha_t'||$ versus the number of stages beyond L for (2,1,6) code. The higher the SNR, the faster the drop.

The proposed TC-MAP decoding algorithm is summarized in Table 1, where $\mathbf{A}^0$ and $\mathbf{A}^1$ are the state transition matrices of the FTB code. As an example, the matrices $\mathbf{A}^0$ and $\mathbf{A}^1$ for the (7,5) code are shown in (5)

$$\mathbf{A}^0 = \begin{bmatrix} 1 & 0 & 0 & 0 \\ 1 & 0 & 0 & 0 \\ 0 & 1 & 0 & 0 \\ 0 & 1 & 0 & 0 \end{bmatrix}, \ \mathbf{A}^1 = \begin{bmatrix} 0 & 0 & 1 & 0 \\ 0 & 0 & 1 & 0 \\ 0 & 0 & 0 & 1 \\ 0 & 0 & 0 & 1 \end{bmatrix} \tag{5}$$

Table 1. Proposed TC-MAP decoding algorithm for FTB codes with block length L and constraint length K.

Inputs:	$\mathbf{A}^0, \mathbf{A}^1, L, P = 2^{K-1}, M = K - 1$
Initialize:	$\boldsymbol{\alpha}_1 = [\frac{1}{P}, ..., \frac{1}{P}]_{1 \times P}, \boldsymbol{\beta}_L = [\frac{1}{P}, ..., \frac{1}{P}]_{P \times 1}^T$
Compute:	from $\gamma_t(s, s')$ with (4) for valid state transitions, normalize $\gamma_t(s, s')$ and store it in $\boldsymbol{\Gamma}_t$ for $t = 1 : L$
	form the row vectors $\boldsymbol{\alpha}_t$ by the forward recursion $\boldsymbol{\alpha}_t = \boldsymbol{\alpha}_{t-1}\boldsymbol{\Gamma}_{t-1}$ and normalize $\boldsymbol{\alpha}_t$ for $t = [2 : L, 1 : M]$
	form the column vectors $\boldsymbol{\beta}_t$ by the backward recursion $\boldsymbol{\beta}_t = \boldsymbol{\Gamma}_t\boldsymbol{\beta}_{t+1}$ and normalize $\boldsymbol{\beta}_t$ for $t = [L - 1 : -1 : 1, L : -1 : L - M + 1]$
	$\mathbf{D}_t^0 = \mathbf{A}^0 \odot \boldsymbol{\Gamma}_t$, and $\mathbf{D}_t^1 = \mathbf{A}^1 \odot \boldsymbol{\Gamma}_t$ for $t = 1 : L$
LLR Output:	$LLR(\hat{b}_t|\mathbf{y}) = ln\frac{\boldsymbol{\alpha}_t\mathbf{D}_t^1\boldsymbol{\beta}_{t+1}}{\boldsymbol{\alpha}_t\mathbf{D}_t^0\boldsymbol{\beta}_{t+1}}$
Hard Decision:	decide $\hat{b}_t = 0$ if $L(\hat{b}_t|\mathbf{y}) < 0$, and $\hat{b}_t = 1$ if $L(\hat{b}_t|\mathbf{y}) > 0$

Despite the similarities of the proposed algorithm to the ones in (Anderson and Hladik, 1998), the proposed circular MAP algorithm for FTBC codes has a fixed wrap-around depth, and less stages for calculating α, β and γ metrics, while achieving similar performance as those in (Anderson and Hladik, 1998). A BER performance comparison is shown in Figure 6 for the same encoder configuration.
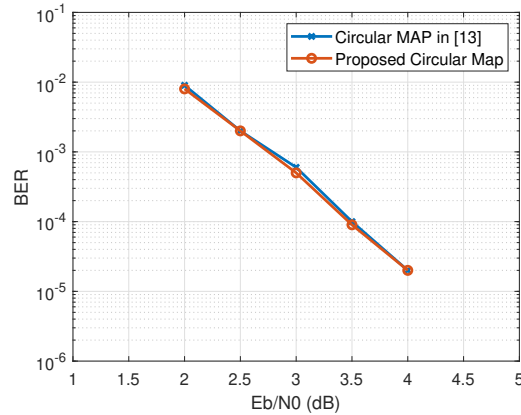
Figure 6. BER of (2, 1, 6) code (554, 744), and $L = 48$ in AWGN channel. Parameters are the same as in (Anderson and Hladik, 1998), Figure 4.

4. SIMULATION RESULTS

This section compares the performance of the three different convolution code techniques using MATLAB simulation. For the PHY-layer performance, each coding technique was simulated in the baseband with different constraint lengths and data block lengths under an AWGN channel. The coding rate was 1/2 and the bit to symbol mapping was BPSK. Constraint lengths were chosen as $K = 3, 6, 9$, and the generator polynomials were (7,5), (74, 64), and (753, 561), respectively. The input data block lengths were $L = 12, 25, 32, 64, 512$. To avoid cluttering in the BER graphs, only the $L = 12$ and the $L = 512$ scenarios are plotted, as shown in Figure 7, where performance of other block

lengths laid in between the two groups of curves. The Direct-Truncation Convolutional (DTC) code was also simulated, where the overhead of the ZTC code was simply discarded without transmission.

The FTBC and ZTC performed very closely to each other, with the performance of FTBC being slightly inferior to the ZTC in all cases. However, the performance gap was only 0.1 dB at BER of 10^{-5}. This demonstrated the advantages of using FTBC as a coding technique for short packets, utilizing 100% of bandwidth without much degradation in reliability. As the constraint length increases, the performance gap between FTBC and ZTC with longer data block lengths was smaller than those with shorter data block length. This is because the traceback length of the decoder is normally $3K$ to $5K$ to achieve good performance. If the data block length is very small, the circular Viterbi algorithm would have insufficient length of the received data to cover the traceback length, thus resulting in some performance loss.

Simulation results for comparison between the MAP and CVA algorithms are shown in Figure 8 for $K = 9$ and $K = 6$. The block length was $L = 64$. The MAP algorithm showed about 0.3 dB better performance than the CVA at BER = 10^{-3}. Other block lengths had similar results which are omitted here. The small performance gain of MAP over CVA is achieved with high computational complexity that involves metrics calculation along the trellis in both forward and backward directions.

For network performance, a slotted-ALOHA network using FTBC or ZTC packets were simulated to study the collision rate of a underwater network. The difference between the short range slotted-Aloha networks for RF and UWA is illustrated in Figure 9, where a node can start a transmission only at the beginning of a time slot, and thus collisions are reduced comparing to a pure-Aloha network. Nodes are located randomly and their distance from other nodes are constrained to $0 < r < R$. The network (a), on the left, demonstrates the relation of the time slot length and the frame size in a RF network. With traveling speed of RF waves being 3×10^8 m/s, the propagation delay T_p is so small that the
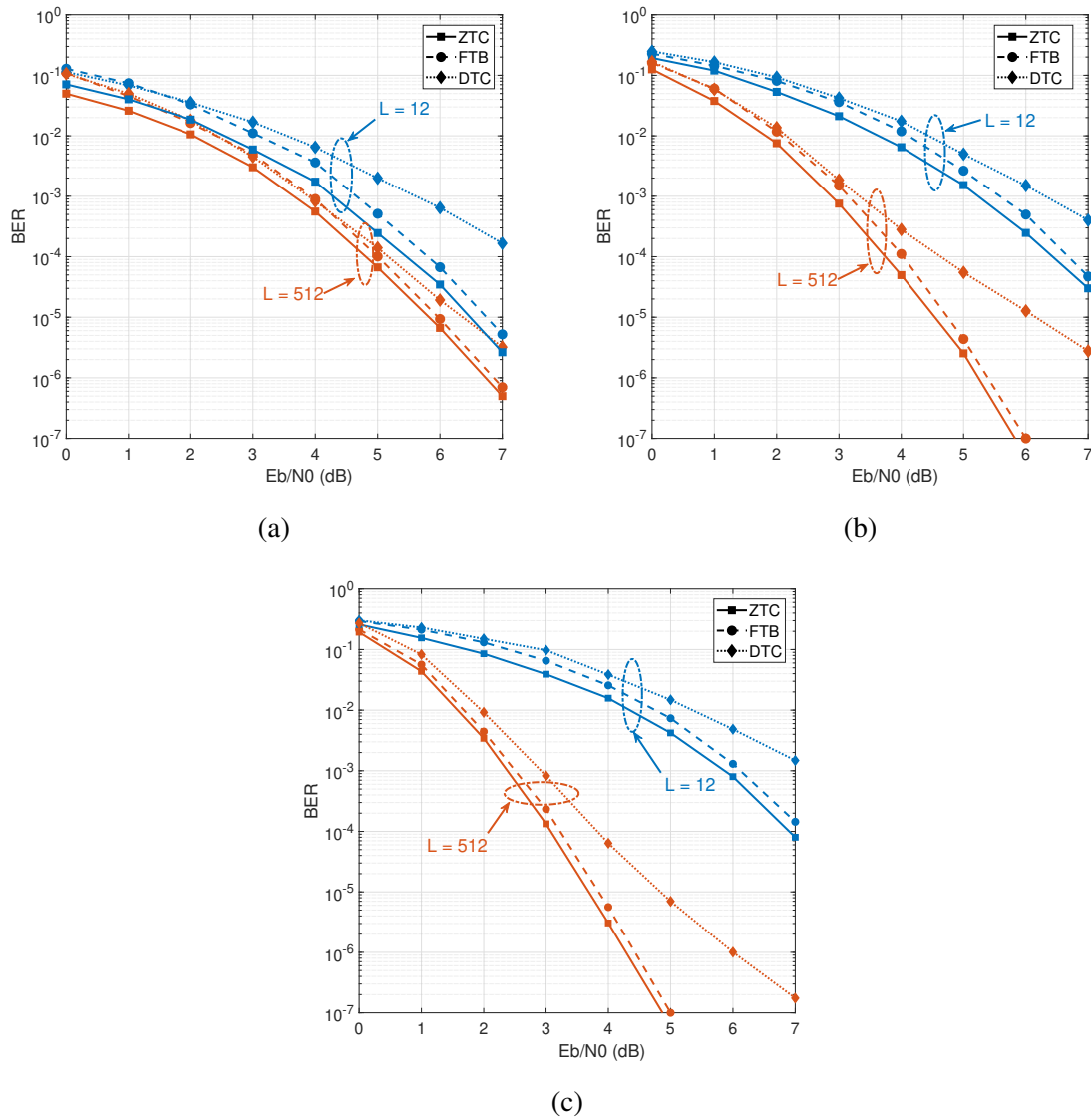
Figure 7. BER performance of CVA in AWGN channels with different constraint lengths: (a) K = 3, (b) K = 6, and (c) K = 9.
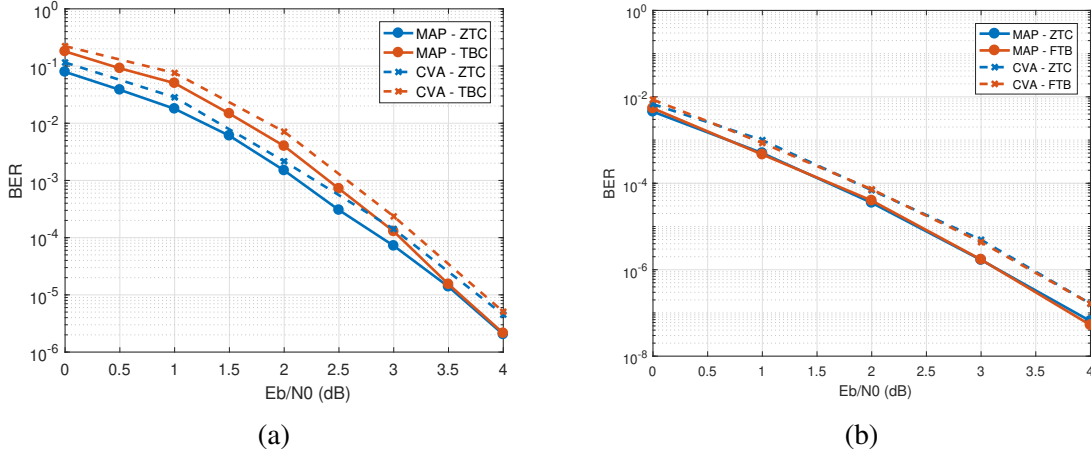
Figure 8. Comparison between TC-MAP and CVA for $L = 64$: (a) $K = 9$, $R = \frac{1}{2}$; (b) $K = 6$, $R = \frac{1}{3}$.

time slot for this network can be set to be equal to the frame size, T_t, and it is proven that the maximum throughput is 1/e frames per frame-time, reached when there is on average one transmission per time slot Chirdchoo *et al.* (2007); De *et al.* (2011). On the other hand, the propagation speed of acoustic waves is about 1.5×10^3 m/s, which is multiple orders of magnitude slower than the RF wave. The propagation delay starts to dominate, especially in ad hoc networks when short messages are exchanged at the network layer. As illustrated in Figure 9 (b), T_p^{max} is the maximal propagation delay between the nodes that have the maximum distance R from each other. The shorter the T_t, i.e. short packets, the stronger the domination of T_p^{max} has on the design of the whole network.

In our simulation, we selected network header parameters similar to the JANUS packet Potter *et al.* (2014), where each header block was 64 information bits which was encoded by a $K = 9$, $R = 1/2$ convolution encoder. JANUS protocol uses the ZTC technique, yielding 144-bits codewords for transmission. The simulation assumed that the channel transmission rate was $R_C = 1$ kbps and acoustic wave propagation speed was $v = 1500$ m/s. In this configuration each JANUS packet was $T_t = 144$ ms in length. In comparison, the FTBC encoded the same 64-bit information block into 128 bits for
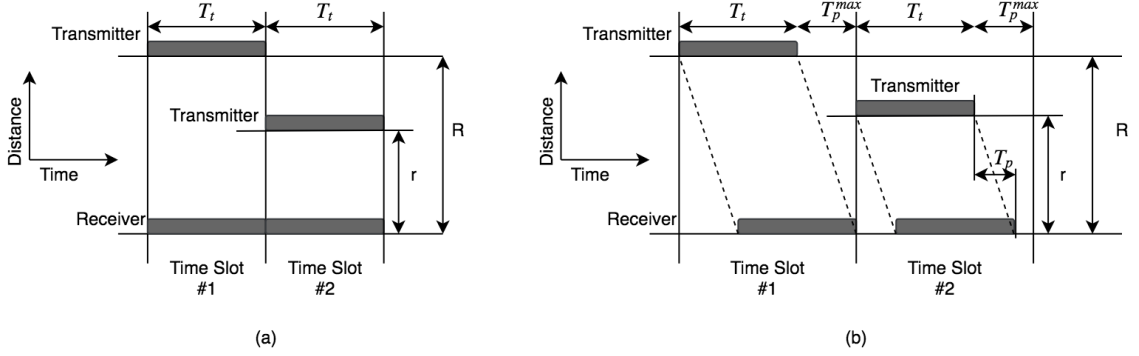
Figure 9. Slotted-Aloha with fixed frame size: (a) RF network, propagation delay is negligible; (b) Underwater acoustic network, propagation delay is comparable to or larger than packet length.

transmission, resulting in 16 ms savings in transmission time. A total of $N = 100$ nodes were scattered randomly in a rectangular area. The nodes were assumed to have homogeneous circular communication range D and the nodes could have any-to-any communications. The transmitters were chosen randomly among the nodes, and each transmitter chose its receiver randomly as well. Note this any-to-any communication scenario is different from the many-to-one simulation used in De *et al.* (2011) where many nodes transmit all to one receive node.

A total of 10^6 packets were transmitted in each simulation trial. A packet collision was detected when any two packets arriving at one receiving node were overlapped in time. Denote the duration of the Aloha time slot as T_{slot} and assume there was at least one node transmitting at the beginning of each time slot. In the first network scenario, we assumed that the maximum propagation time was less than the packet transmission time. That is $T_p^{max} < T_t$. The 100 nodes were placed randomly in a 100×100 m^2 area where $T_p^{max} = 94.3$ ms. With T_{slot} ranging from 150 ms to 200 ms, the collision rates dropped quickly as T_{slot} was increased, as shown in Figure 11. Note that, in both ZTC and FTBC packet types, the same number of information bits per time slot was transmitted. When $T_{slot}/(T_t + T_p^{max}) \approx 85$ %, the collision rate for ZTC approached 10^{-3}. On the other hand, by only changing the
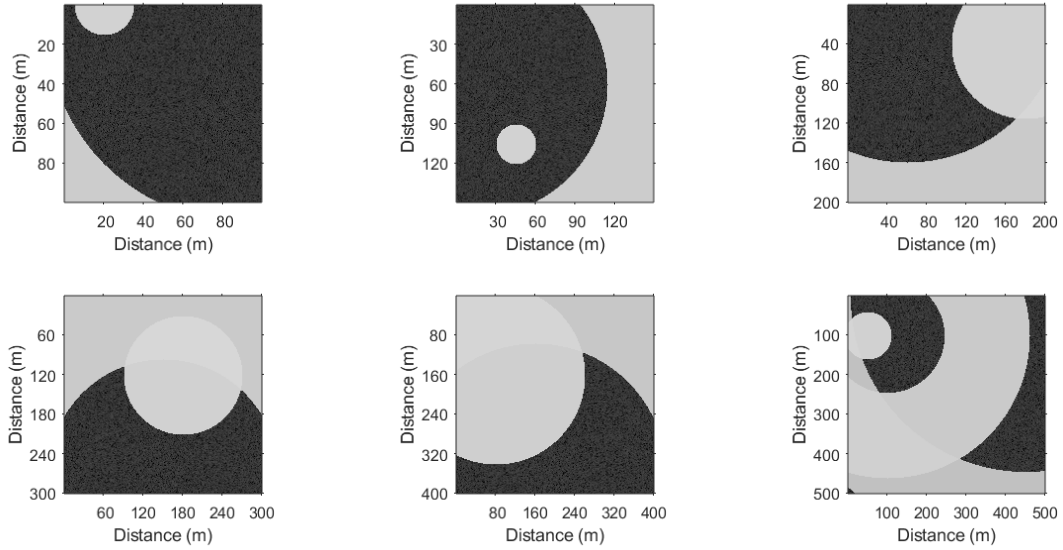
Figure 10. Snapshots of UWN scenarios at a given time. Each ring or disc represents an acoustic wave generated by a transmitter at the center propagating outwards. Bright gray scale indicates the power received at that point. The maximum communication distance was $D = 5000$ m.

encoding technique to FTBC, the network reduced the collision rate to 10^{-5}. This is over two orders of magnitude improvement in effective throughput of the network, as shown in Figure 11 (a).

In the second network scenario, we assumed a constant $T_{slot} = 200$ ms, and the packet collision rate was simulated based on increasing the area that the 100 nodes occupied. The domination of T_p^{max} started to grow as the network area increased. The simulation results in Figure 11 (b) demonstrates that when T_p^{max} became longer than the packet duration, the packet collision rate increased dramatically for both types of encoding. Nevertheless, the FTBC outperformed ZTC in all cases. Although the packet collision rate was high as 40-50% in a large T_p^{max} scenario, the network throughput was still a lot higher than that of the many-to-one network simulated in De *et al.* (2011) as the transmission rate was as high as
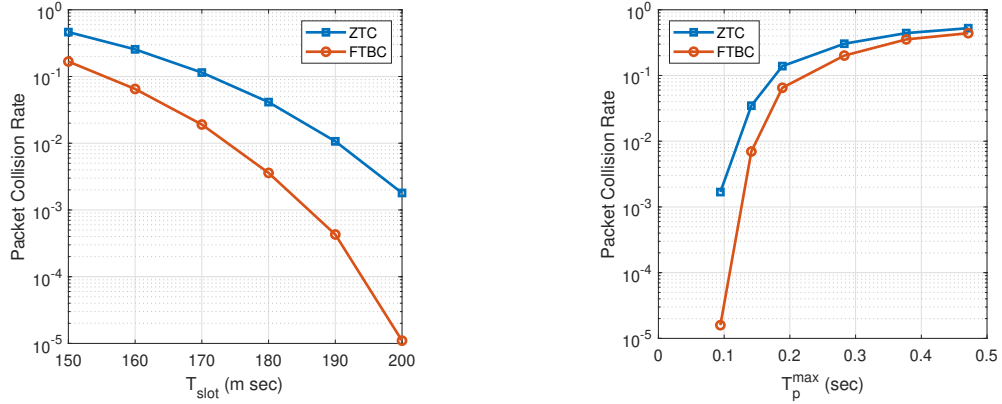
Figure 11. The packet collision rates in a slotted-Aloha network where T_{slot} is the duration of a slot time. Unlike the networking protocol in Figure 9 where $T_{slot} = T_t + T_p^{max}$, our simulation chose a T_{slot} smaller than the sum $T_t + T_p^{max}$.

one packet per time slot. Based on the results in Figure 11, we conclude that network packet collision reduces as the length of transmitted packets becomes shorter, and the benefit is most significant when the maximum propagation delay is less than packet duration.

Another underwater network scenario was simulated to demonstrate the bandwidth efficiency of the FTBC codes compared to the ZTC codes, where 100 IoT devices communicating with a base station was considered. The base station transmitted 10,000 packets to a randomly chosen IoT device and each packet contained 64 information bits including IoT device address, packet number, payload, and a cyclic redundancy check (CRC) bit. The communication channel was randomly selected from the watermark channel library van Walree *et al.* (2016) which were time-varying and frequency selective underwater acoustic channels measured by real-world ocean experiments. Figure 12 demonstrates two examples of such channels used in the simulation. The information blocks were encoded by the constraint length $K = 9$ FTBC or ZTC, and the data rate was $R_b = 1$ kbps. Upon a reception, an IoT device decoded the packet with the MAP algorithm and checked for any remaining errors using the CRC. A negative acknowledgement (NACK) was sent back to the base station upon error detection and the NACK also served as an automatic repeat request (ARQ). The NACK packet was a 32-bits packet containing IoT device address, packet number, and
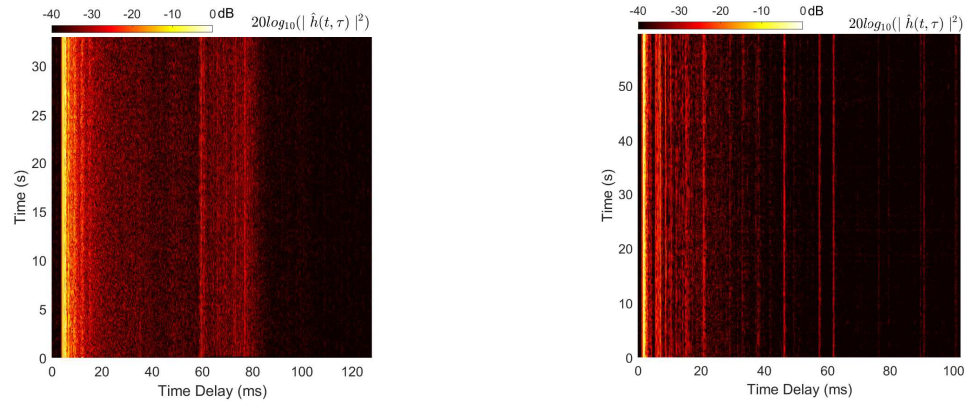
Figure 12. Two samples of watermark channels used in the simulation.
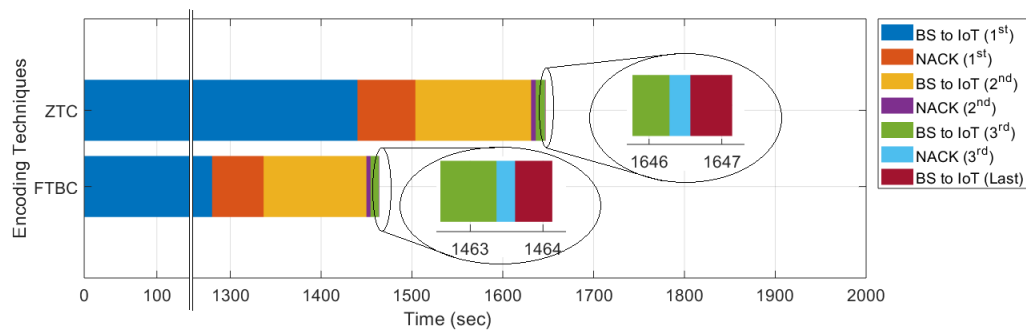
Figure 13. Comparison of the performance of a network using ZTC, FTBC as their encoding technique. FTBC completes 10000 packet transmission approximately 180 seconds earlier than ZTC.

CRC, encoded with the same coding technique. For the simplicity of the simulation, the NACK packets were assumed to reach the base station with no errors. Upon receiving the NACK, the base station re-transmitted the requested packets until ARQ was received. The total time in successfully transmitting the 10,000 information packets, as well as the NACK, or ACK, is demonstrated in Figure 13, where the network utilizing the FTBC code took less time to reach the throughput than the ZTC codes and over 11% time savings was achieved, which translated to 11% improvement of network efficiency.

Different codes and modulation schemes were designed for the experiment. Unfortunately, due to various physical constraints, only two test cases recorded valid data. One was the frame with constraint length $K = 6$ and code rate of $R = 1/3$, another was $K = 9$ with $R = 1/2$. Both cases used the On-Off Keying (OOK) modulation scheme. OOK has the advantage in IoT applications in that it simplifies the carrier demodulation without the need of carrier phase synchronization. The SNR performance of OOK would be slightly lower than the BPSK, but the synchronization overhead is reduced which further shortens the packet length. The generator polynomials used in these two cases were $G_6 = [75, 53, 47]$, and $G_9 = [753, 561]$, respectively. The data block lengths that are fed to the encoders are the same as simulation. The coded data rate was $R_b = 2560$ bps, and the baseband signal was pulse-shaped using a square-root-raised-cosine (SRRC) filter with a sampling rate of $f_s = 10240$ Hz. Finally, the baseband waveform was modulated by the modem with a carrier frequency of $f_c = 18560$ Hz, and a bandwidth of $BW = 4160$ Hz. The LFMB frequency range was $f_c - R_b < f < f_c + R_b$ Hz.

The examples of the received passband signals are shown in Figure 15, after being passed through a bandpass filter centered at f_c. An impulsive interference, also shown in Figure 15, corrupted some of the recordings. Those portions of the received signal were identified and discarded from the data analysis.
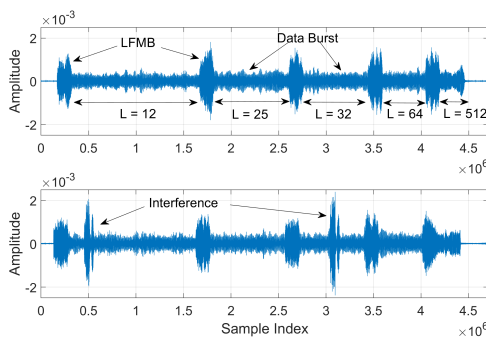
Figure 15. Received passband signals after a bandpass filter. The impulsive interference was from an unintended transmitter near the receiver.

Received signal is then demodulated non-coherently, by passing through an envelope detector and an square-root raised cosine (SRRC) filter. Frame and symbol synchronization was achieved by correlating the LFM with the received signal to find the starting point of the data stream. Figure 16 shows a normalized output of the correlation, where Figure 16(a) shows the peaks for the whole frame with each peak indicating the start of a new data block. This synchronization method was rather coarse and was very sensitive to multipath fading channels since multiple correlation peaks were produced and the first peak might be lower than the later peaks under non-minimum phase channels, as shown in Figure 16(b). Fine synchronization for symbols was achieved by the minimum mean square error method using the first block of data, as shown in Figure 16(b). The highest peak in Figure 16(b) was the start of the frame and the first symbol.
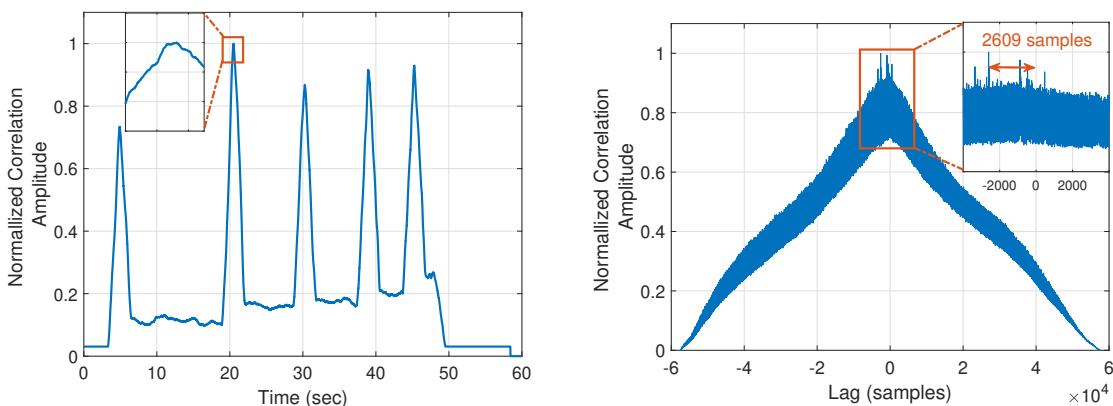
Figure 16. Correlation of LFMB with received OOK signal (a) coarse synchronization in a frame; (b) fine synchronization via MMSE.

The multipath channel impulse response of one block was estimated using the transmitted data. A 3D bi-time representation of channel magnitude response is depicted in Figure 17 for a complete transmission frame. It is clear that the total multipath duration was about 50 ms, and the time variation of the channel was severe with an estimated maximum Doppler frequency of 3.1 Hz, which yields to 50% coherence time of $T_c = \sqrt{\frac{9}{16\pi f_m^2}} \approx 136$ ms Rappaport (2001).
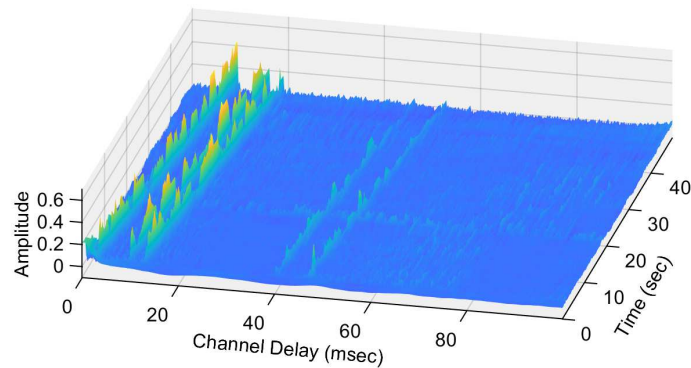
Figure 17. Bi-time representation of the fading channel magnitude response.

Zooming in to 20 seconds of channel impulse response, the amplitude response of the multipath channels are shown in Figure 18, where each subplot was the estimated channel with a time lapse of 2 seconds apart. The strong multipath arrivals were mostly in the first 15 – 20 msec of the channel impulse response with 3-5 high-amplitude paths, followed by a small cluster at 40 msec, then another low-amplitude cluster at 60 - 80 msec. The strong paths in the first cluster may be separated by a few msec in time, which allowed the short data blocks to be received without ISI. This observation confirms that the BER performance of short blocks may be better than those of the long blocks when no channel equalizer was used.
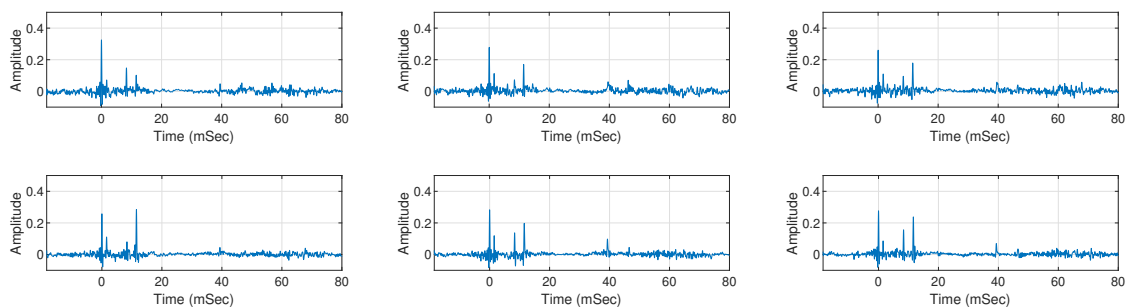
Figure 18. Channel impulse response (amplitude response) estimated form ocean experiment.

The down-sampled baseband signals were decoded by CVA and TC-MAP decoders. Finally the decoded bits are compared to the transmitted data to estimate the BER. The total numbers of processed bits are listed in Table 2 for the (2,1,8) code and (3,1,5) code. The error probabilities are plotted in Figure 19. Without channel equalizer, the short data blocks performed very well in both subfigures. With the (3,1,5) codes, the ZTC achieved $3.5 \times 10^{-3}, 7 \times 10^{-3}, 1.5 \times 10^{-2}$ for $L = 12, 25, 32$, respectively. The FTBC short data blocks also achieved comparable error rate with $6 \times 10^{-3}, 1.1 \times 10^{-2}, 1.6 \times 10^{-2}$ for $L = 12, 25, 32$, respectively. The DTC clearly suffered from performance loss with the short data blocks with $1.5 \times 10^{-2}, 1.8 \times 10^{-2}, 2.5 \times 10^{-2}$ for $L = 12, 25, 32$, respectively. For longer data blocks such as $L = 64$ and $L = 512$, the three convolutional coding schemes performed similarly with high errors due to ISI caused by the severe multipath channels. Similar results are shown for the (2,1,8) codes.

Table 2. Total number of processed bits for each scenario.

	12	25	32	64	512
$K = 9, R = 1/2$	26880	35000	37888	47104	44032
$K = 6, R = 1/3$	19200	19000	29696	27648	27648

With the estimated noise power at each block, the signal to noise ratio (SNR) of each data block was estimated and the blocks with similar SNRs were grouped together. The average SNR of each group was then calculated and plotted as the x-axis for the BER plots in Figure 20 and Figure 21, which are BERs for the (2,1,8) code and the (3,1,5) code, respectively. In all cases, the ZTC had the best performance, compared to other techniques, especially for the very short data blocks of $L = 12$. With SNR as low as 2-6 dB, the length 12 ZTC achieved BER below 10^{-2} in both (2,1,8) and (3,1,5) codes. The FTBC codes performed moderately worse than the ZTC but a lot better than the DTC. It is interesting to note that, for the (3,1,5) FTBC codes, the length 25 case performed better than the length 12 case at almost all SNRs. This was because the data block length of the $L = 25$ FTBC was short enough to avoid most multipath interference and long enough to obtain error
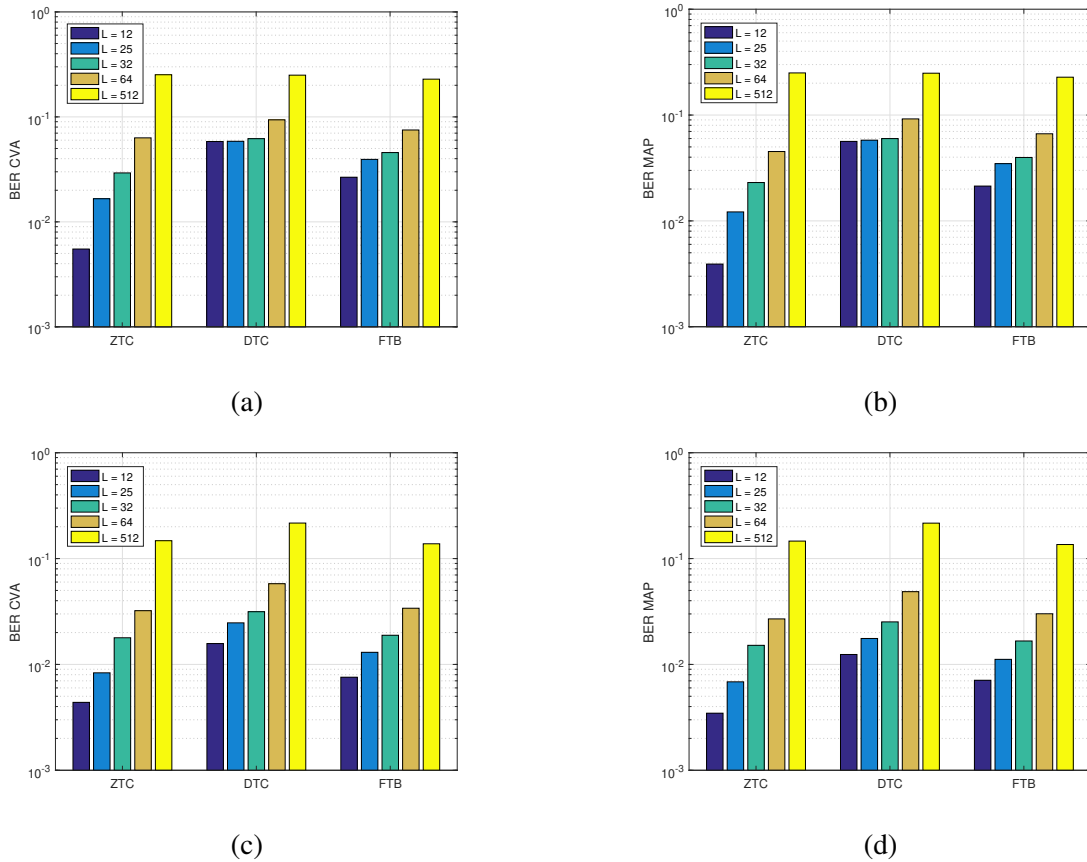
Figure 19. Total bit error performance comparison. (a) CVA results for (2,1,8) code, (b) TC-MAP results for (2,1,8) code, (c) CVA results for (3,1,5) code, (d) TC-MAP results for (3,1,5) code.

correction capability. In all cases, the shorter the packet the better the performance. The reason for that is, the shorter packets were less contaminated by the extended multi-path property of UWA channel.

6. CONCLUSION

In this paper, we proposed a new tail-biting circular MAP decoder with low computational complexity, and evaluated its performance for tail-biting convolutional codes for very short data blocks in underwater acoustic communications for both PHY, and MAC layers. The lengths of the data blocks are 12, 25, 32, 64 and 512, and the (2,1,8) and (3,1,5) FTBC
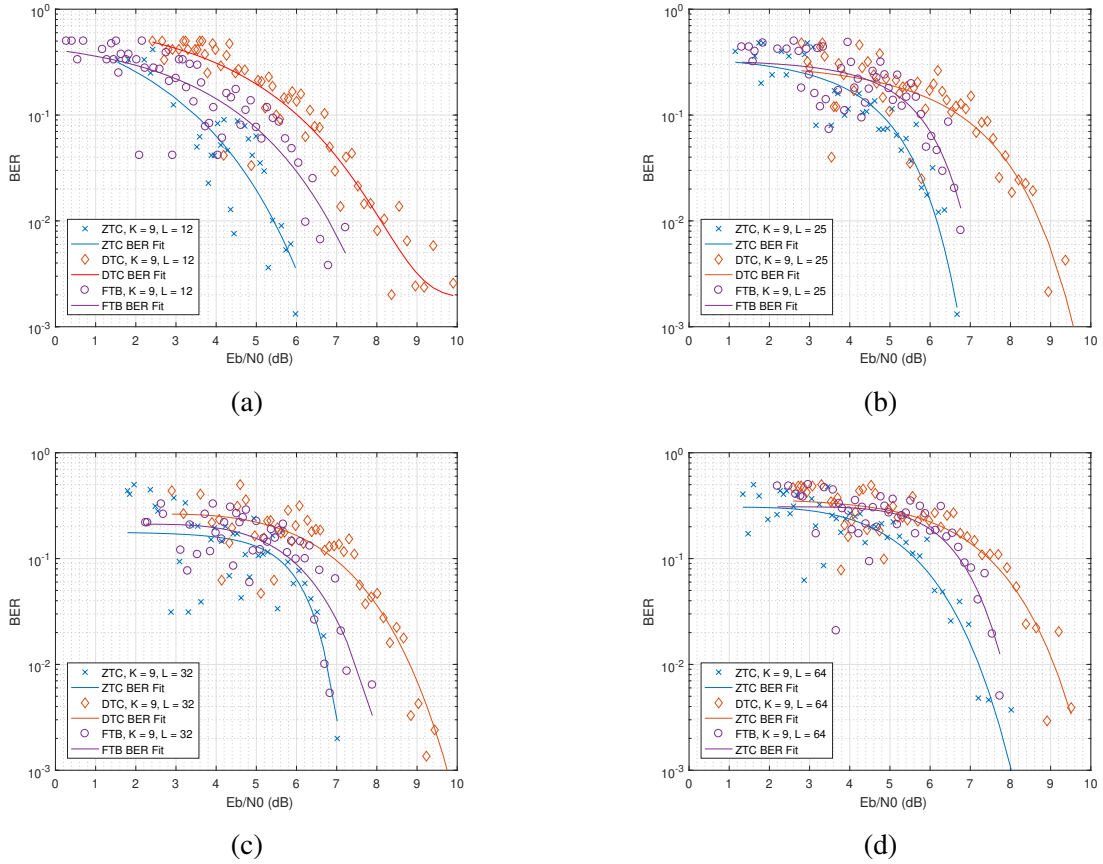
Figure 20. TC-MAP BER curves with estimated SNR for (2,1,8) code from ocean experiment. (a) $L = 12$, (b) $L = 25$, (c) $L = 32$, (d) $L = 64$.

codes are compared with the ZTC codes. The ocean experimental results show that without channel equalization, FTBC codes with short packet lengths not only can perform similar to ZTC codes, in terms of BER, they can outperform the ZTC codes in terms of collision rate, and bandwidth utilization in a massive network of battery powered IoT devices, that cannot afford to use complex and power-consuming equalization algorithms. These results provide interesting suggestions that the short data blocks may suffer less from inter-symbol interference, induced by the multipath fading channels, and form packet collision; and a strong channel code alone can be effective for communication of short data blocks over underwater acoustic channels.
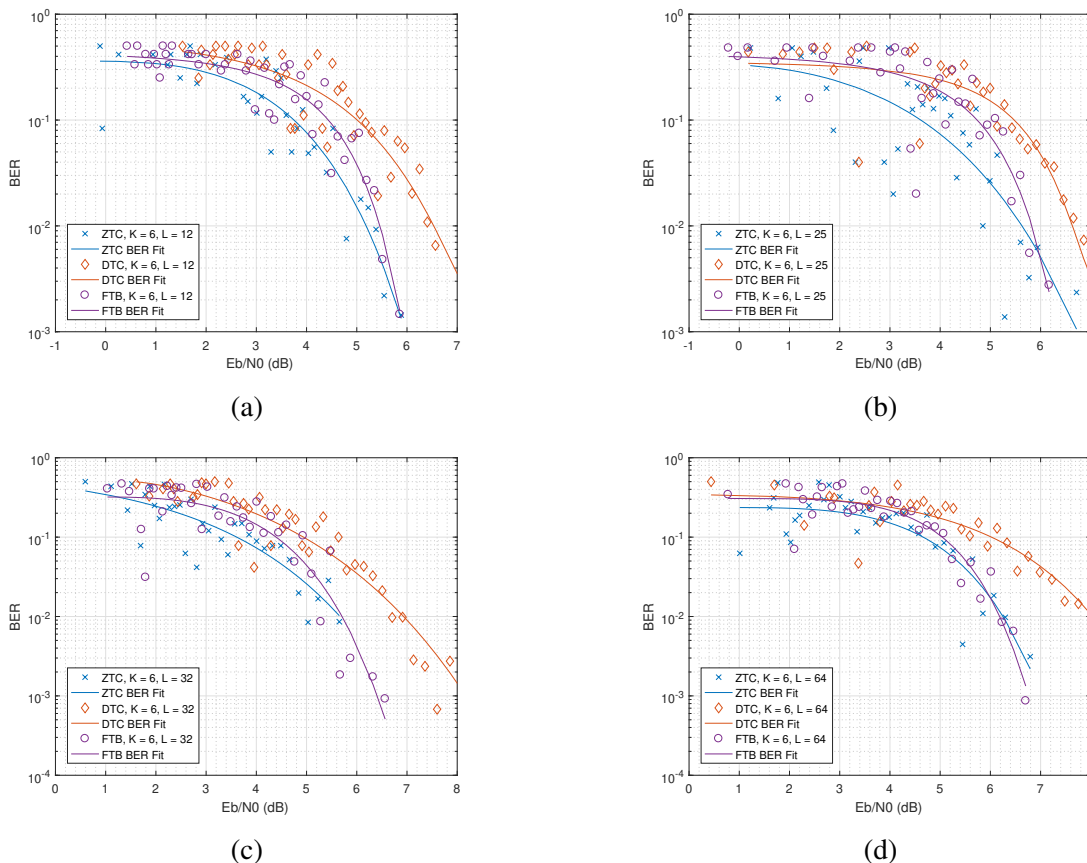
Figure 21. TC-MAP BER curves with estimated SNR for (3,1,5) code from ocean experiment. (a) $L = 12$, (b) $L = 25$, (c) $L = 32$, (d) $L = 64$.

REFERENCES

Anderson, J. B. and Hladik, S. M., 'Tailbiting map decoders,' IEEE Journal on Selected Areas in Communications, 1998, **16**(2), pp. 297–302.

Anderson, J. B. and Hladik, S. M., 'An optimal circular viterbi decoder for the bounded distance criterion,' IEEE Transactions on Communications, 2002, **50**(11), pp. 1736–1742.

Bahl, L., Cocke, J., Jelinek, F., and Raviv, J., 'Optimal decoding of linear codes for minimizing symbol error rate (corresp.),' IEEE Transactions on information theory, 1974, **20**(2), pp. 284–287.

Behgam, M., Zheng, Y. R., and Liu, Z., 'Coding for short messages in multipath underwater acoustic communication channels,' in 'OCEANS 2018 MTS/IEEE Charleston,' ISSN 0197-7385, 2018 pp. 1–5, doi:10.1109/OCEANS.2018.8604711.

Boccardi, F., Heath, R. W., Lozano, A., Marzetta, T. L., and Popovski, P., 'Five disruptive technology directions for 5g,' IEEE Communications Magazine, 2014, **52**(2), pp. 74–80.

Chirdchoo, N., Soh, W. ., and Chua, K. C., 'Aloha-based mac protocols with collision avoidance for underwater acoustic networks,' in 'IEEE INFOCOM 2007 - 26th IEEE International Conference on Computer Communications,' ISSN 0743-166X, 2007 pp. 2271–2275, doi:10.1109/INFCOM.2007.263.

Chitre, M., Shahabudeen, S., and Stojanovic, M., 'Underwater acoustic communications and networking: Recent advances and future challenges,' Marine Technology Society Journal, 2008, **42**(1), pp. 103–116.

Clark Jr, G. C. and Cain, J. B., *Error-correction coding for digital communications*, Springer Science & Business Media, 2013.

Cox, R. V. and Sundberg, C.-E. W., 'An efficient adaptive circular viterbi algorithm for decoding generalized tailbiting convolutional codes,' IEEE transactions on vehicular technology, 1994, **43**(1), pp. 57–68.

De, S., Mandal, P., and Chakraborty, S. S., 'On the characterization of aloha in underwater wireless networks,' Mathematical and Computer Modelling, 2011, **53**(11), pp. 2093 – 2107, ISSN 0895-7177, doi:https://doi.org/10.1016/j.mcm.2010.06.041.

Domingo, M. C., 'An overview of the internet of underwater things,' Journal of Network and Computer Applications, 2012, **35**(6), pp. 1879 – 1890, ISSN 1084-8045, doi: https://doi.org/10.1016/j.jnca.2012.07.012.

Durisi, G., Koch, T., and Popovski, P., 'Toward massive, ultrareliable, and low-latency wireless communication with short packets,' Proceedings of the IEEE, 2016, **104**(9), pp. 1711–1726.

Han, Y., Wu, T.-Y., Chen, P.-N., and Varshney, P., 'A low-complexity maximum-likelihood decoder for tail-biting convolutional codes,' IEEE Trans. Communications, 2018, **PP**(99), pp. 1 – 1.

Lin, S. and Costello, D. J., *Error control coding*, Pearson Education India, 2004.

Liva, G., Gaudio, L., Ninacs, T., and Jerkovits, T., 'Code design for short blocks: A survey,' arXiv preprint arXiv:1610.00873, 2016.

Ma, H. and Wolf, J., 'On tail biting convolutional codes,' IEEE Transactions on Communications, 1986, **34**(2), pp. 104–111.

Potter, J., Alves, J., Green, D., Zappa, G., McCoy, K., and Nissen, I., 'The janus underwater communications standard,' 2014 Underwater Communications and Networking, UComms 2014, 2014, doi:10.1109/UComms.2014.7017134.

Raghavan, A. R. and Baum, C. W., 'A reliability output viterbi algorithm with applications to hybrid arq,' IEEE Transactions on Information Theory, 1998, **44**(3), pp. 1214–1216.

Rappaport, T. S., *Wireless Communications: Principles and Practice*, Prentice Hall PTR, 2001.

Shao, R. Y., Lin, S., and Fossorier, M. P., 'Two decoding algorithms for tailbiting codes,' IEEE transactions on communications, 2003, **51**(10), pp. 1658–1665.

Stojanovic, M. and Preisig, J., 'Underwater acoustic communication channels: Propagation models and statistical characterization,' IEEE Communications Magazine, 2009, **47**(1), pp. 84–89, ISSN 0163-6804, doi:10.1109/MCOM.2009.4752682.

van Walree, P., Otnes, R., and Jenserud, T., 'Watermark: A realistic benchmark for underwater acoustic modems,' in '2016 IEEE Third Underwater Communications and Networking Conference (UComms),' 2016 pp. 1–4, doi:10.1109/UComms.2016.7583423.

Viterbi, A., 'Error bounds for convolutional codes and an asymptotically optimum decoding algorithm,' IEEE Trans. Inform. Theory, 1967, **13**(2), pp. 260 – 269.

Wang, Q. and Bhargava, V. K., 'An efficient maximum likelihood decoding algorithm for generalized tail biting convolutional codes including quasicyclic codes,' IEEE transactions on communications, 1989, **37**(8), pp. 875–879.

Williamson, A. R., Marshall, M. J., and Wesel, R. D., 'Reliability-output decoding of tailbiting convolutional codes,' IEEE Transactions on Communications, 2014, **62**(6), pp. 1768–1778.

Zheng, Y. R., Wu, J., and Xiao, C., 'Turbo equalization for single-carrier underwater acoustic communications,' IEEE Communications Magazine, 2015, **53**(11), pp. 79–87, ISSN 0163-6804, doi:10.1109/MCOM.2015.7321975.

II. PASSBAND DATA REUSE OF FIELD EXPERIMENTAL DATA IN UNDERWATER ACOUSTIC COMMUNICATIONS

Mohammadhossein Behgam, Xiangzhao Qin, Yahong Rosa Zheng, *Fellow, IEEE*

ABSTRACT

This paper expands the passband data reuse approach, first proposed by Deane, Preisige and Singer in UCOMM 2018, to utilize the underwater acoustic (UWA) wireless communication signals acquired in a real-world experiment as a tool for evaluating new coding and modulation schemes in realistic doubly spread UWA channels. The passband data reuse approach first finds the differences in coding and modulation schemes between the original experimental scheme and the new scheme under test (SUT), then modifies the baseband signals in both the transmitter and receiver while keeping the passband transmit and receive signals unchanged. This paper provides detailed procedures of the passband data reuse method for testing the SUTs that change or add error correction coding, change bit to symbol mapping (baseband modulation) schemes with a set of original experimental data. The passband data reuse approach is compared to three existing approaches: one is the direct field experiment approach which is costly; one is the baseband direct channel playback approach that uses the estimated baseband equivalent channel impulse response (CIR) from an experimental data, and the third one is the computer channel simulation approach that generates baseband fading CIRs with Wide-Sense Stationary Uncorrelated Scattering (WSSUS) approximation. The performance of the passband data reuse approach is similar to the direct field experiment approach; while the performance of the baseband direct channel playback approach is similar to the WSSUS channel simulator approach. We conclude that under specific conditions, the time-varying and non-stationary characteristics

of the real-world UWA channels are preserved by the passband data reuse approach and the performance of the new SUT evaluated by the passband data reuse approach can be considered as under the similar conditions as the original experiment scheme.

Keywords: Acoustic communications, field experiment, data reuse, underwater fading channels, non-stationary scattering, channel modeling.

1. INTRODUCTION

Underwater acoustic (UWA) communications channels lack explicit models that could capture the underlying physics of ocean telemetry and characterize the time varying doubly spread nature of channels (Kilfoyle and Baggeroer, 2000). Therefore, many researchers in the field of UWA communications still require sea-going measurement campaigns to evaluate their transmitter and receiver algorithms (van Walree *et al.*, 2008). Holding these campaigns to acquire field data is often expensive, time consuming, and prone to many types of failures (Deane *et al.*, 2018). Besides these difficulties, the acquired field data are often privately protected in individual research groups, and most probably the data will be left unused after the funded research activity is completed. However, due to the lack of readily and publicly available channel models, joining the sea-going campaigns has remained the only opportunity that a researchers could evaluate newly proposed algorithms (Stojanovic and Preisig, 2009).

To reduce the cost of extensive field experiments, researchers in the field of UWA communications have proposed many models and simulators for acoustic communication channels in the past decades. Often the proposed models include a few assumptions, approximations, and simplifications over key parameters of acoustic waves propagation in the ocean (Bjerrum-Niese and Lutzen, 2000; Kilfoyle and Baggeroer, 2000). These parameters include, but are not limited to, wide or quasi-wide sense stationarity, sound speed profiles, sea floor compositions and roughness, time-delay, frequency dispersion,

noise or multipath characteristics, etc. These assumptions, although applicable to a specific case or scenario, often lack the knowledge for prediction and evaluation of true long-term ocean channel models.

Alternatively, the baseband direct channel playback approach is proposed in (van Walree *et al.*, 2008), which uses the baseband equivalent channel impulse response (CIR) estimated from some original experimental signals to replace the computer simulated CIRs. The SUT is first demodulated to baseband and convolved with the estimated CIRs, then re-modulated to the passband to yield the received signals of the SUT. This approach may capture the time-varying nature of the CIR by updating the adaptive estimation in a fine time scale, but still suffers from the fact that the true passband channel was not experience by the SUT but a Wide-Sense Stationary Uncorrelated Scattering (WSSUS) approximation of the channel.

Recently, an interesting approach was proposed by Deane, Presig and Singer (Deane *et al.*, 2018) to preserve the passband transmitted and received signals from a field experiment, but modify the baseband signals to test the SUT by finding the difference between the original baseband signal and the SUT at the transmitter and then add the difference in the received baseband signals. The authors call it post-experiment modification. We rename this approach passband data reuse in this paper. While the work in (Deane *et al.*, 2018) described hard decoding and symbol detection schemes of the passband data reuse approach, we provide detailed procedures for the receiver soft decision decoding, soft symbol detection, and Turbo equalization. We also evaluate the passband data reuse approach against the direct field experiment approach using SPACE 08 experimental data, as well as the direct channel playback approach, and the computer channel simulation approach. Our results show that the passband data reuse approach performed similarly to the field experiment approach, allowing the researchers to reuse the recorded signals from previously successful experiments to evaluate different communication signaling schemes in an actual real-world scenario, but with fractional cost of the field experiment. In comparison, the

direct channel playback approach performed similarly to the computer simulation approach. The SUT under the simulated channels and direct channel playback method achieved better BERs than the passband data reuse approach and the field experiment approach, indicating significant performance gaps.

2. EXISTING CIR SIMULATION AND DIRECT CHANNEL PLAYBACK

2.1. COMPUTER SIMULATION MODELS

UWA channel simulation may be achieved by two methods: one is acoustic wave theory-based simulation; one is the stochastic CIR generation. The wave theory-based simulation utilizes ray tracing to model the physical wave propagation from the transmitter to the receiver. The related tools include Bellhop (Porter, 2019), Karen (Peterson and Porter, 2013), and parabolic equation method (Song *et al.*, 2011), etc. The key computation of ray-tracing models is the integration of the ray approximation to the acoustic wave equation with respect to time. The eigenrays represent the paths through the sound channel from the source to a receiver by tracing the rays radiating from the source (Peterson and Porter, 2013). The time varying ray-tracing algorithms simulate channels by providing a complex valued amplitude $C_i(t)$ to reflect the varying phase changes regarding each ray interacting with sea floor and sea surface. The delay time τ_i expresses the observed channel by the receiver for each eigenray $i = 1, ..., N$. Then the observed channel by the receiver can be written as the sum of the N eigenrays (Siderius and Porter, 2008) given by

$$y(t) = \sum_{i=1}^{N} C_i(t)x(t - \tau_i).$$

The ray-tracing based simulator has the advantage of being able to map ocean environment parameters, such as temperature, salinity, wind, air bubbles, and sound profiles, etc., into the channel responses. It is also capable of simulating shadow zones in underwater channels.

However, the wave theory-based computer simulators suffer from high computational complexity if time-variation and randomness are incorporated in the simulation. The stochastic CIR simulators include the sum of sinusoids method (Zheng and Xiao, 2003), the Markov chain method, and the Doppler spectrum filtering method (Qarabaqi and Stojanovic, 2013). Experimental channel measurements demonstrate different distributed behaviours such as Rice, or Rayleigh (Chitre, 2007), or compound K-distributed (Yang and Yang, 2006) highly dependent on the environment. Therefore, computer simulation models for these probability distributions of fading envelops are also developed. The power density spectrum of the fading process is the standardized U-shape Doppler spectrum which is derived from the WSSUS assumption. The computer simulation approach has the advantage of generating CIRs with independent or correlated multipath and Doppler spread properties, as well as low computational complexity. However, unlike in a terrestrial radio channel where the WSSUS assumption is well accepted, underwater channel models often experience non-stationary scattering. It is difficult to find an accepted statistical model of acoustic communication channels (Stojanovic and Preisig, 2009).

2.2. DIRECT CHANNEL PLAYBACK

In contrast to the pure computer simulation, the direct channel playback simulators estimate the time-varying CIRs using field experimental data (van Walree *et al.*, 2017). Given a set of ocean experimental data, the transmitted signals are treated as channel probe signals and received signals are carrier demodulated to baseband. The baseband equivalent CIRs are estimated with shifted time windows of the received signals to yield time-varying CIRs $h(\tau, t)$ which is a function of delay time τ, and time t. To apply the direct channel playback to a SUT, the passband signal of the SUT is first demodulated to baseband, then convolved with the baseband CIRs, and re-modulated back to passband. Hence, the simulator replays the field experimental channel through a tapped delay line or FIR filter

with taps T_s seconds apart,

$$y(t) = \sum_{k=0}^{K} b_k(t)x(t - kT_s) \tag{1}$$

where T_s is the sampling interval and the tap gains $b_k(t)$ can be obtained by

$$b_k(t) = \int_{-\infty}^{\infty} h(\tau,t)\text{sinc}\left(\frac{\tau - kT_s}{T_s}\right).$$

This is obtained based on the assumption that the waveform is band-limited with bandwidth BW and $T_s < 1/BW$. However, $h(\tau,t)$ is tracked at a lower rate and the simulator linearly interpolates the channel taps between each tracking for simulation purposes (van Walree *et al.*, 2008). Thus, the time varying underwater acoustic channels are considered quasi-WSSUS, meaning that the channel behaves like a WSSUS channel for short and restricted time intervals. As long as the channel tracking rate is well above its fading rate, the direct channel playback approach works fine (Socheleau *et al.*, 2015; van Walree *et al.*, 2008). Figure 1 demonstrates the block diagram of the direct channel playback simulator.
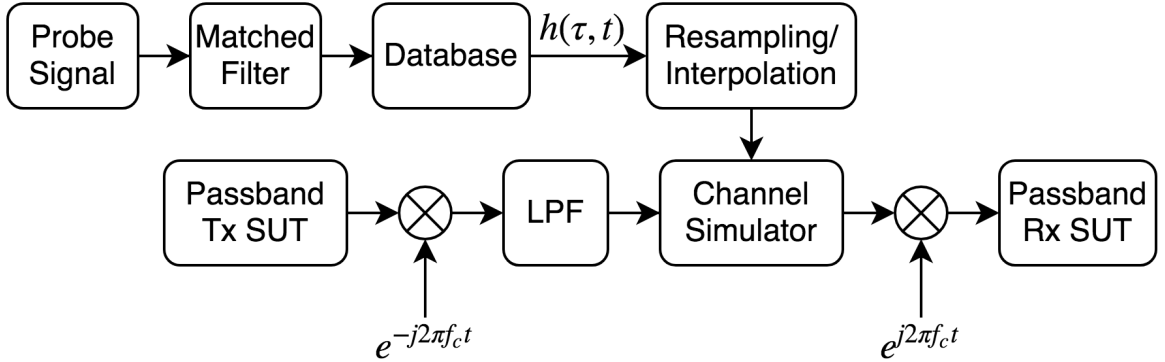
Figure 1. Block diagram of direct channel playback simulator. PRBS probe signals is used to estimate the time varying channel impulse response using matched filtering method to be used in channel playback simulator.

The direct playback simulators enjoy the low computational complexity and the flexibility of using different ocean experimental data. On the other hand, the drawback arises from the fact that the simulated channel is quasi-WSSUS, especially when the channel tracking rate is a lot lower than its sampling rate, then the simulators upsample the measured

channels and linearly interpolate the channel taps from one tracking to another. We will see in Section 4 that, this method performs, on average, 10 dB better than the field experiment approach, thus cannot fully represent the dynamics of a real-world underwater channel.

3. PASSBAND DATA REUSE

Consider a general Single-Input Single-Output (SISO) underwater acoustic communication system illustrated in Figure 2. In the original experiment, a bit stream b_n generated from a source is passed through the forward error correction encoder and the interleaver to generate the c_n bit stream. Then, the coded bits in c_n are grouped and mapped to symbols via an M-ary digital modulation scheme. Finally, the symbols are upsampled, pulse-shaped, and modulated with the carrier $e^{j2\pi f_c t}$. The real part of the modulated output is the signal $x(t)$ that is transmitted in the original experiment.

In order to use the signals received in the original experiment and test new coding algorithms, a different bit stream b'_n is generated from a random source, encoded and interleaved by by the new coding/interleaving algorithms of the SUT to generate c'_n. At this stage, the mapping between c'_n and c_n bit streams must be obtained to yield m_n in Figure 2. This can be achieved by passing the two bit streams through an XOR block, as long as $length(c_n) \geq length(c'_n)$.

A general signal flow diagram of the receiver architecture is demonstrated in Figure 3, to enable the reuse of the passband field experimental data. Let $y(t)$ be the received passband signal in the original experiment. It is first demodulated via the commonly-used algorithms, including bandpass filtering, carrier demodulation with $e^{j2\pi f_c t}$, matched filtering downsampling, and possibly channel equalization. The soft de-mapper calculates the log-likelihood ratio (LLR) of each individual bit from the symbols of the original experiment, i.e. $LLR(\hat{c}_n)$. At this stage, a Soft XOR block is proposed to convert the $LLR(\hat{c}_n)$ to $LLR(\hat{c}'_n)$ designed for post experiment. This block uses the mapping m_n

obtained in the transmitter to calculate the $LLR(\hat{c}'_n)$ by

$$LLR(\hat{c}'_n) = (-1)^{m_n} LLR(\hat{c}_n) \tag{2}$$

Equation (2) enables the utilization of soft-output soft-input algorithms such as turbo equalization and MAP decoding by reserving the confidence in the output of soft de-mapper $LLR(\hat{c}_n)$, and just changing the sign to map the $LLR(\hat{c}_n)$ to $LLR(\hat{c}'_n)$. After the LLR of the SUT is obtained, the de-interleaver and the decoder of the SUT are used to process the post experiment data and evaluate the performance of the SUT.
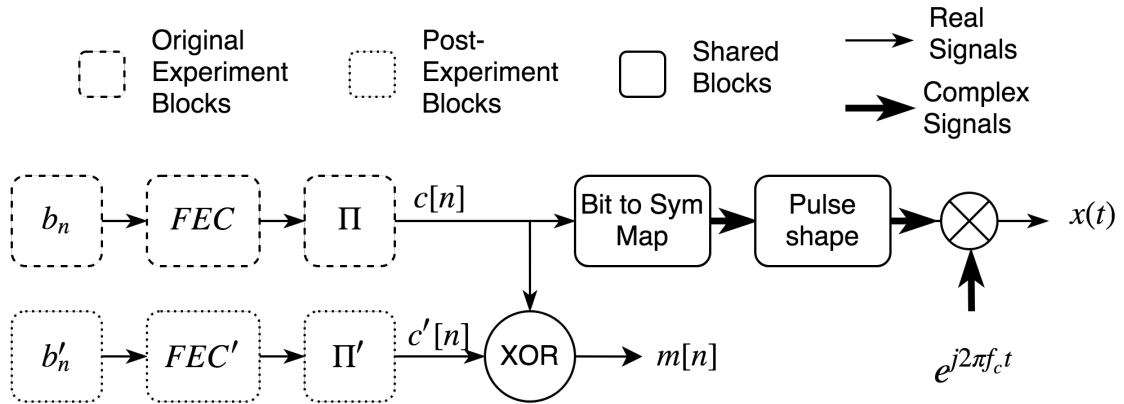
Figure 2. Block diagram of transmitter. Signal flow is demonstrated for original experiment and passband data reuse. In this diagram the original and post experiment signal flow are different in source, encoder, and interleaver blocks.
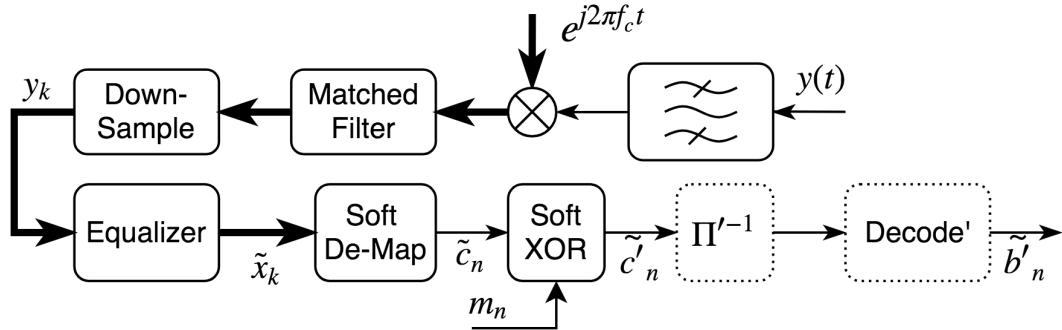
Figure 3. Receiver block diagram and signal flow for passband data reuse.

Common bit-to-symbol mapping used in wireless communications are PSK (Phase Shift Keying) and QAM (Quadrature Amplitude Modulation). In scenarios where lower order modulation is desired than what is available in the original experiment this procedure can be used in combination with constellation reduction (CR) block, demonstrated in Figure 4, where an 8-PSK is mapped to a QPSK (Quadrature PSK).

Constellation reduction block combines the gray coded neighboring symbols that contain a number of common bits to generate a new symbol that could represent all the symbols in their region. An M-PSK mapping scheme is written as

$$s_n = \exp\left(j\left(\frac{2\pi n}{M} - \phi_0\right)\right), \ n = 0, 1, 2, ..., M - 1 \tag{3}$$

where ϕ_0 is the initial phase offset of the constellation. CR block can reduce a higher order M-PSK to a lower order M'-PSK, by

$$s_n' = \exp\left(j\frac{\pi}{M}(-1)^{\left\lfloor \angle s_n - \theta \right\rfloor \frac{M'}{\pi}}\right)s_n \tag{4}$$

where $\theta = \pi/M - \phi_0$.

An example of 8PSK constellation points generated by (3) and reduced to QPSK using (4) is demonstrated in Figure 5. In this constellation, the least significant two bits that are common between each neighboring symbols decide the new QPSK symbol regions.
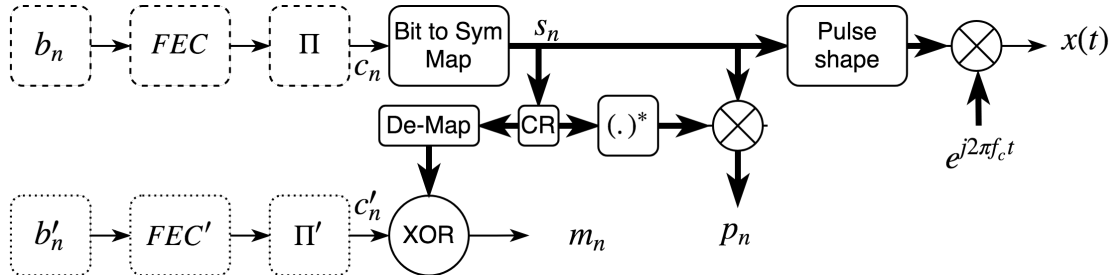
Figure 4. Transmitter block diagram and signal flow for constellation order reduction post experiment.
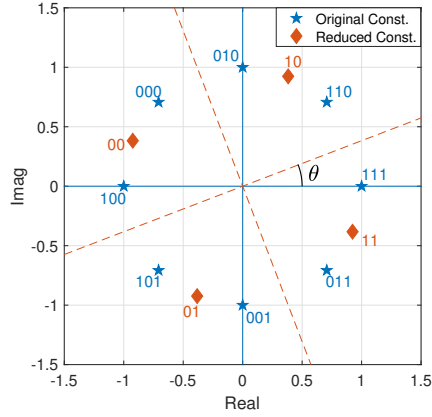
Figure 5. Phase shift keying constellation reduction. In this figure an 8PSK constellation is reduced to QPSK.

Constellation points in an M-QAM mapping scheme can be obtained by

$$s_n = \sum_{m=1}^{\log_2 \sqrt{M}} \sqrt{\frac{M}{2^{2m-1}}} \exp\left(j\frac{\pi}{4}\left(4b_{2m-1} + 2b_{2m} + 1\right)\right) \tag{5}$$

where the bs are the $\log_2 M$ bits grouped together to generate the symbol s_n and $\log_2 \sqrt{M} \in \mathbb{Z}$. Equation (5) describes the M-QAM constellation points as a summation of $\log_2 \sqrt{M}$ vectors rotating in $\log_2 \sqrt{M}$ circles with radius proportionate to $\sqrt{M/2^{2m-1}}$. Figure 6 demonstrates the generation of 64-QAM constellation points using (5). The CR block can reduce a higher order M-QAM to a lower order M'-QAM by (6) where $q = \log_2 \sqrt{M/M'}$.

After Constellation is reduced, it is necessary to obtain the mapping p_n between the previous higher order modulation symbols to the new symbols that contains the phase and amplitude offset information by $p_n = s'_n/s_n$, demonstrated in Figure 4. Using this mapping, the random phase and amplitude offsets can be removed from the received signal right before equalization, as demonstrated in Figure 7. New symbols s'_n generated as a result of constellation reduction have to be de-mapped into bits, in order to obtain the mapping m_n between the new bit stream and the c'_n stream, generated for post experiment using the XOR operation.
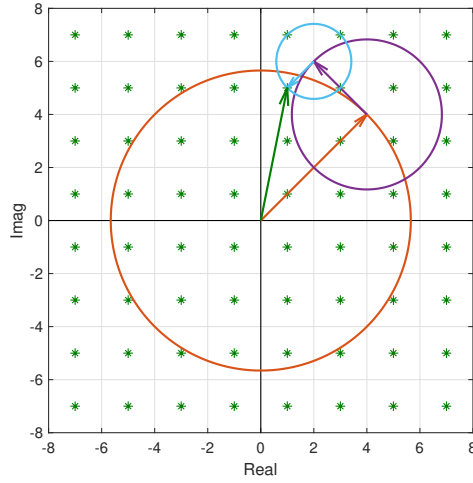
Figure 6. Quadrature amplitude modulation constellation order reduction. In this figure a 64QAM is reduced to 16QAM.

$$s'_n = \left(s_n - \sum_{m=\log_2 \sqrt{M}-q}^{\log_2 \sqrt{M}} \sqrt{\frac{M}{2^{2m-1}}} exp\left(j\frac{\pi}{4}\left(4b_{2m-1} + 2b_{2m} + 1\right)\right)\right)\Big/2^q \tag{6}$$

4. PERFORMANCE RESULTS AND ANALYSIS

In this section we validate the idea of reusing previous underwater acoustic communications experiments to test new algorithms designed for transmitter and receiver. We also compare this method to direct channel replay simulators to see how accurately each method can represent real-world underwater acoustic channel scenarios.

Recorded signals from an undersea trial of SPACE08 (Tao *et al.*, 2010) are used to validate the idea of reusing previous underwater acoustic communications experiments in order to simulate real-world underwater acoustic channels. We first evaluate the bit error rate performance of the original experiment to have a common ground to compare other
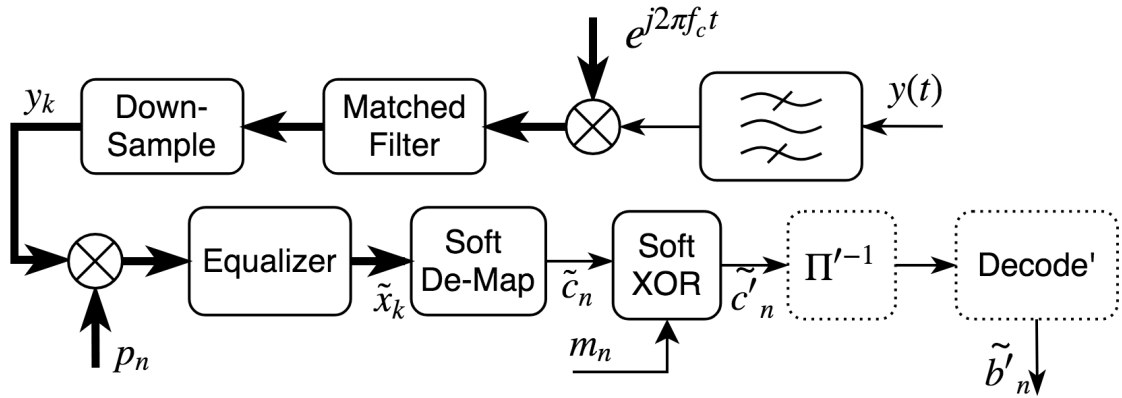
Figure 7. Receiver block diagram and signal flow constellation order reduction post experiment.

coding and decoding scenarios. We then use the method proposed in this paper to test four different post experiment scenarios. Finally, we compare the results with the outcome of direct channel playback simulator.

The undersea trial, SPACE08, was conducted at the coast of Martha's Vineyard, Edgartown, MA, in October 2008. In this experiment, convolutional code with constraint length 4 and code rate of 1/2, combined with a random interleaver was used on the transmitter side. Total of 30000 symbols was generated for each digital baseband modulation scheme, i.e. QPSK, 8PSK, 16QAM, with symbol period of T_s = 0.1024 ms, and the carrier frequency was f_c = 13 kHz, with sampling frequency f_s = 39.0625 kHz. The single carrier modulation frame structure, shown in Figure 8, was adopted for transmission, where the data frame consisted of a header, three data packets, and a tail. The header and tail of the transmitted signal were LFMB and LFME, respectively, each having a 1000-symbol length of linear frequency modulation (LFM) signal surrounded by some gaps. The header and tail were for Doppler estimation, frame synchronization, and carrier synchronization purposes.

For receiver block diagram we have adopted a channel-estimation based turbo equalizer (Tüchler and Singer, 2011) (CT-TEQ), shown in Figure 9. This receiver incorporates improved proportionate normalized least mean square (IPNLMS) as channel estimation

LFMB	Gap	QPSK packet	8PSK packet	16QAM packet	Gap	LFME
1000	300	31200	31200	31200	300	1000

m-seq.	Gap	Data payload	Gap
511	189	30,000	500
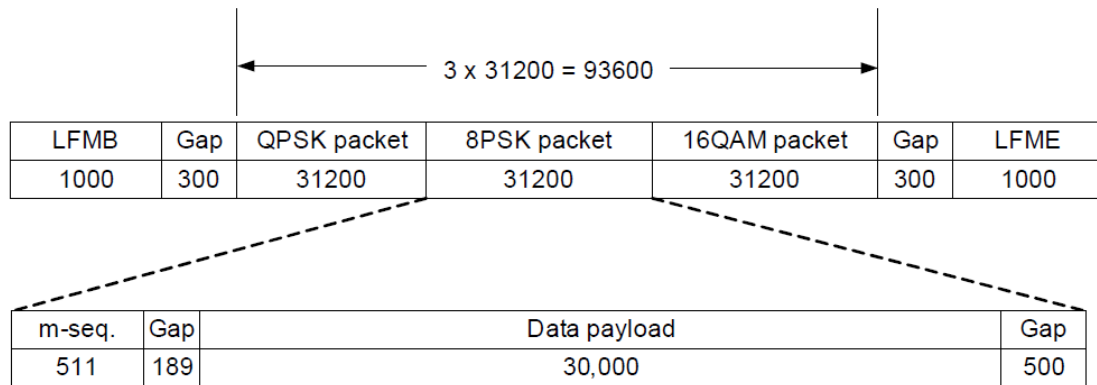
Figure 8. Transmitted signal frame structure in space08.

method combined with maximum *a Posteriori* (MAP) decoder to boost the performance of the equalizer (Yang and Zheng, 2016), demonstrated in Figure 9. This equalizer explicitly estimates the channel coefficients using pilot sequence and then adapts to changes in channel condition while decoding the information bits (Tao *et al.*, 2010).
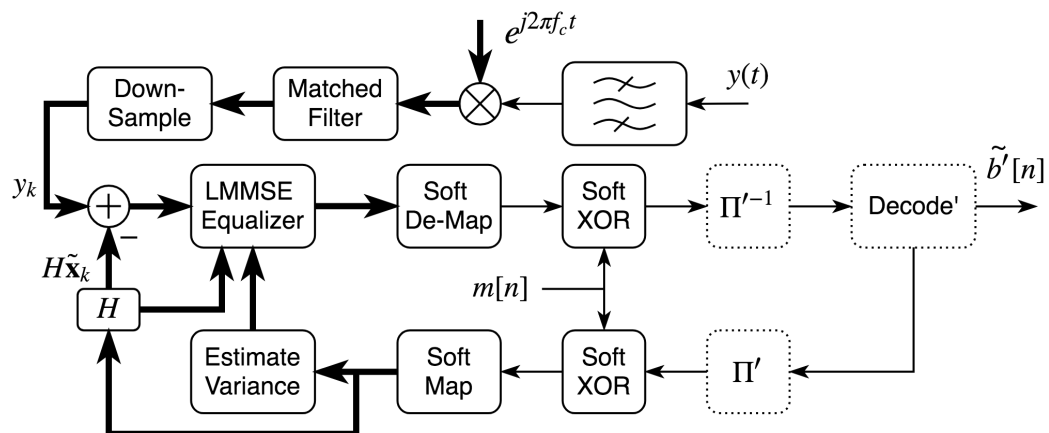
Figure 9. Turbo equalizer receiver block diagram and signal flow.

A simulation was designed to compare the performance of direct channel playback simulator and actual signal transmission. Rician channel with $Kfactor = 1.5$, and maximum Doppler shift of 2 Hz was used with the multipath properties illustrated in Figure 10 with a 3 dB loss associated with each bottom reflection. Same generated channel is

used in two ways. First, a pseudorandom binary sequence (PRBS) signal is used as a probe signal. Passband BPSK signal with symbol interval of T_{sym} = 0.1024 ms, and the carrier frequency was f_c = 13 kHz, with sampling frequency f_s = 39.063 kHz is generated using the probe signal and passed through the generated Rician channel. In order to estimate the time varying impulse response (TVIR) of the channel, to be used in direct channel playback simulator, the received signal is demodulated to baseband and matched filtered by the baseband representation of PRBS signal. Figure 10 illustrates a sample estimated impulse response and doppler spectrum of channel. Then the desired transmission signal is fed to the simulator along with the estimated TVIR to generate the received signal. In the second way, the desired transmission signal is passed directly through the same Rician channel. The packet error rate performance comparing these methods is shown in Figure 10(d), where the direct channel playback simulator demonstrates better BER performance than experimental evaluation and the passband data reuse. This indicates that the direct channel playback approach predicts the upper bound of the performance.

In order to perform the direct channel playback simulation the coherence time of all received packets was estimted to be approximately 0.21 < T_c < 0.44 seconds in worst and best cast scenario. Then channel was assumed quasi-WSSUS and tracked every 30 ms and the impulse response is estimated using MMSE algorithm based on the transmitted baseband waveform. A sample estimated channel impulse response is shown in Figure 11. The replay filter upsamples the tracking rate of the estimated channel to match it to the sampling rate of the received signal and then the channel variation between each tracking is linearly interpolated. Comparing the original experiment results with direct playback simulator results, demonstrated in Figure 12 for QPSK, 8PSK and 16QAM, respectively, shows that this method does not capture all the effects of a UWA channel and BER performance is unrealistically better than the original experiment.
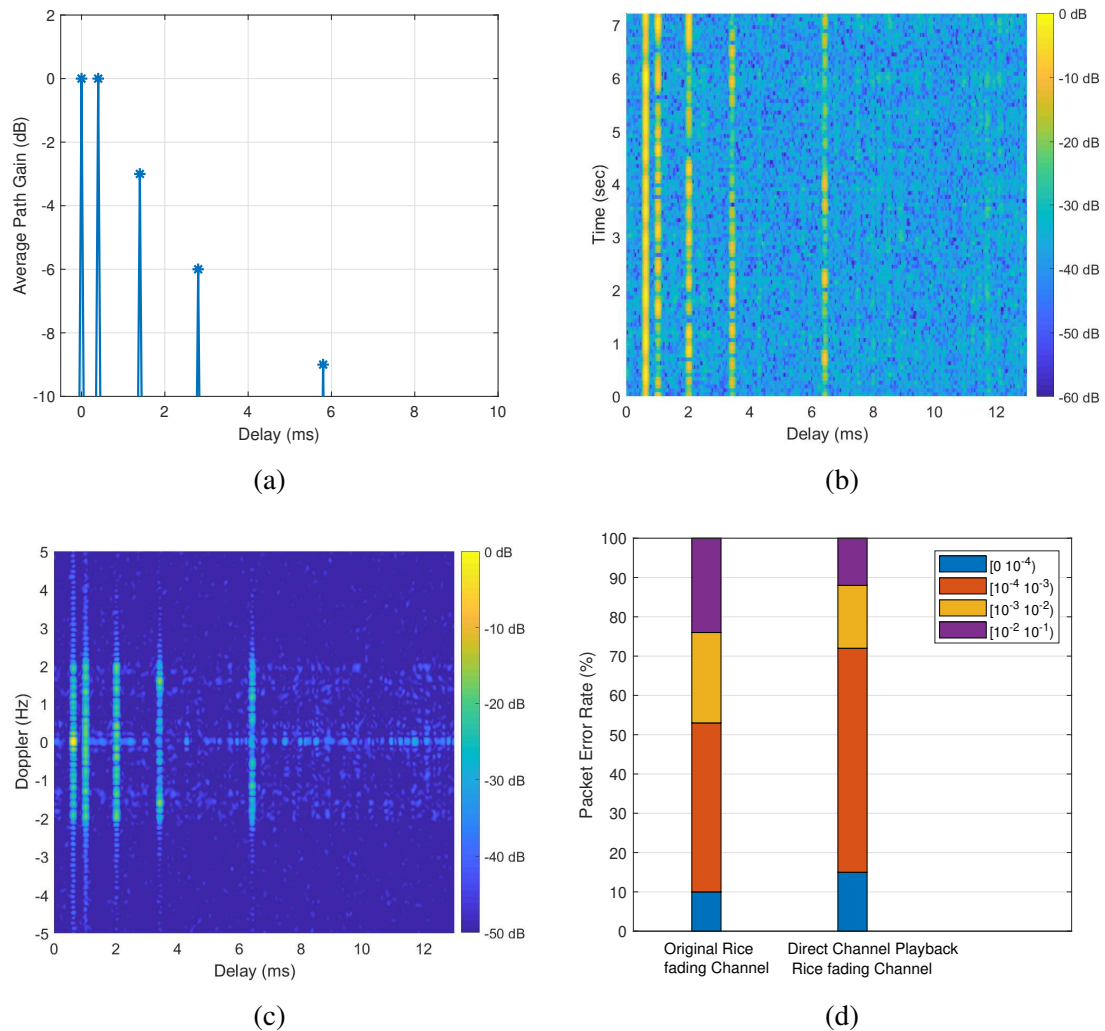
Figure 10. Multipath properties of underwater acoustic channel generated for direct playback simulator for a system operating near bottom of the sea. (a) overall magnitude response of channel, (b) Time varying Rician channel impulse response generated for simulation, (c) Doppler spread of the channel, (d) Packet error rate comparison of the simulated Rice fading channel with direct channel playback simulator of same channel.

To validate whether the proposed method could simulate a realistic UWA channel two post-experiments were designed in which convolutional encoders were used as an FEC, like the original experiment. However, post-experiment 1 uses convolutional encoder with constraint length 6 and post-experiment 2 uses one with constraint length 3. It is expected that post-experiment 1 will have a better BER performance and post-experiment 2 will have
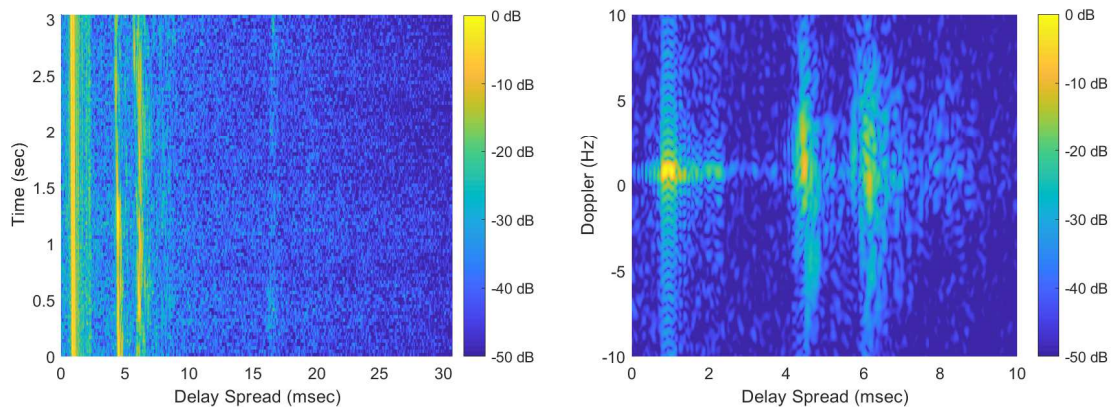
Figure 11. Multipath properties of underwater acoustic channel for SPACE08. (a) Estimated time varying impulse response, (b) Estimated Doppler spread of channel
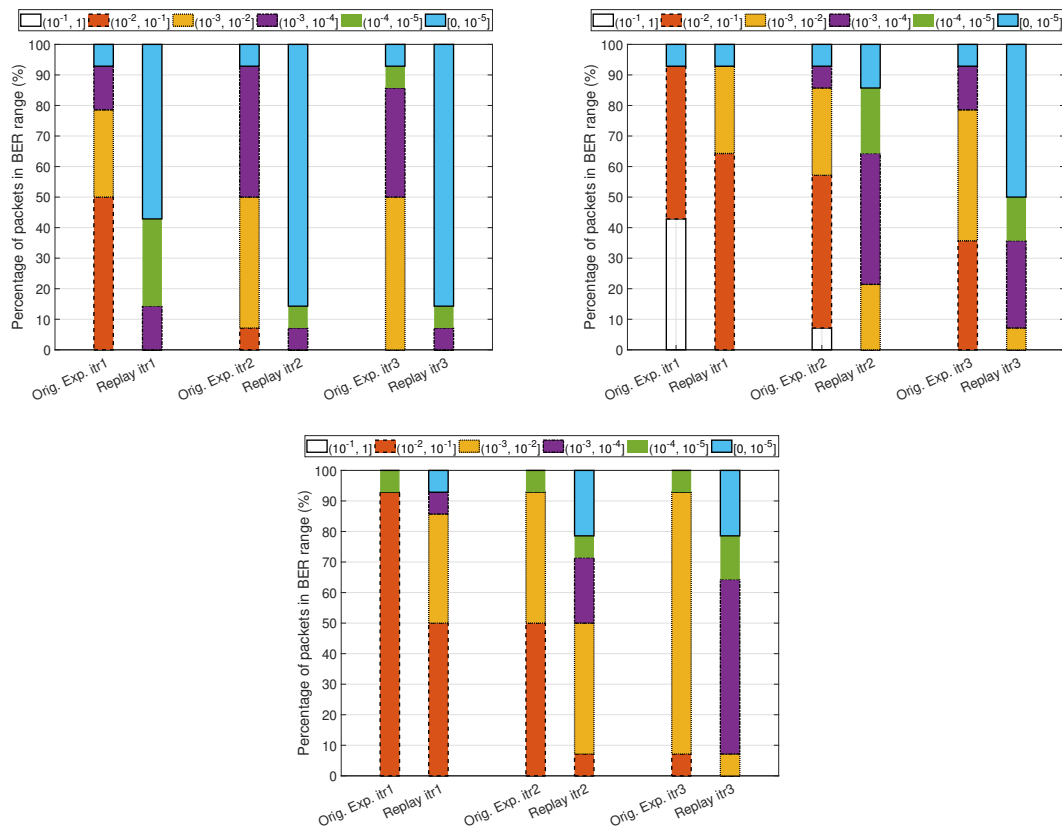
Figure 12. Packet error performance comparison of SPACE08 experiment with channel playback simulator using turbo equalizer. In all three iterations of detection channel playback simulator demonstrates better performance than original experiment.

slightly worse BER performance than original experiment. Figure 13 which demonstrates the result of turbo equalization algorithm after 3rd iteration for QPSK, 8PSK, and QAM 16, respectively, confirms our expectations.

(a) QPSK

(b) 8PSK

(c) 16QAM
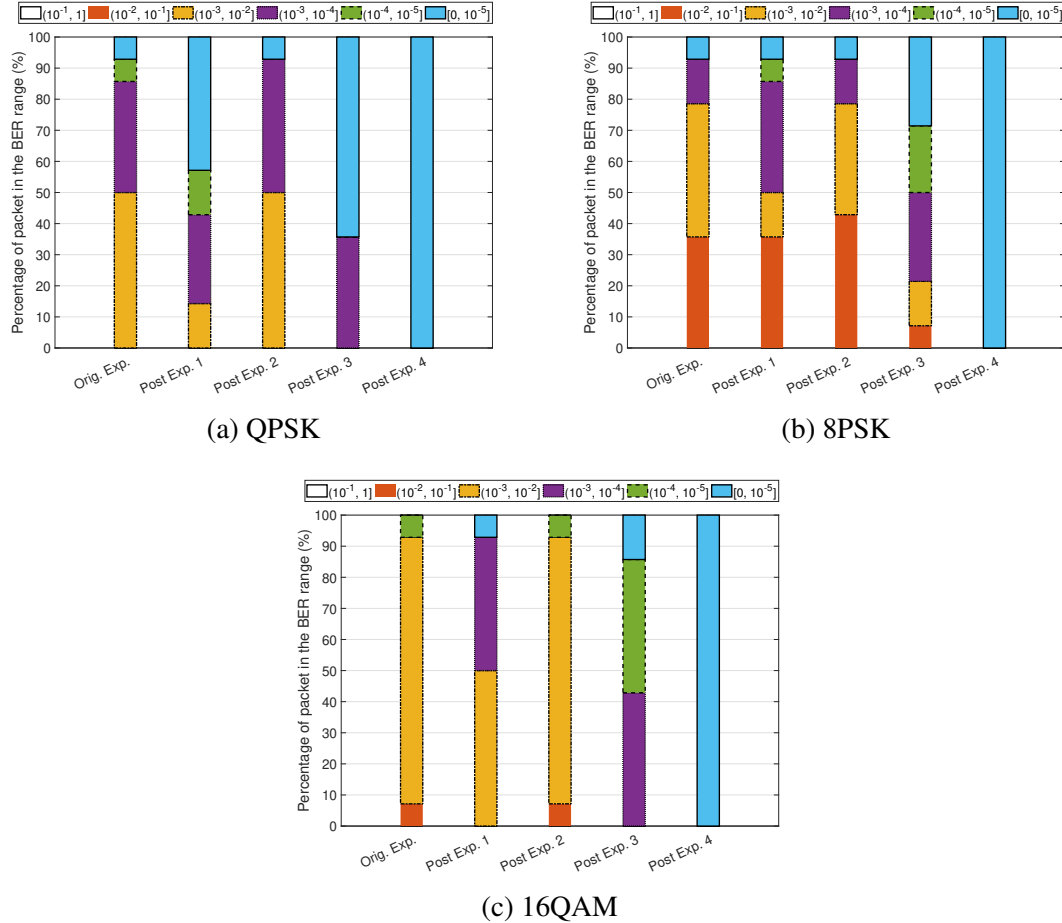
Figure 13. Packet error performance comparison of SPCAE08 experiment and four post experiments designed to test the passband data reuse.

Another two post-experiments were designed with completely different types of FECs. Post-experiment 3 uses LDPC encoder and decoder in the transmitter and receiver, respectively. The LDPC code can be denoted as $(n, w_c, w_r) = (nSym \log_2 M, 6, 7)$ is used in this test, where n is the code length, w_c is the column weight, and w_r is the row weight, $nSym = 30000$ is the total number of symbols, and M is the order of mapping scheme. BER performance for post-experiment 3 is shown in Figure 13.

The post-experiment 4 tests a turbo encoder made out of a parallel concatenated coding scheme with constraint length 4, code generator [13, 15], and feedback connection on polynomial 13. The receiver uses the block diagram demonstrated in Figure 3 with the iterative decoding scheme that uses the a posteriori probability (APP) decoder as the constituent decoder, an interleaver, and a deinterleaver. BER performance for the post-experiment 4 are also shown in Figure 13 after 3 iterations of decoding.

To test whether the proposed method of reusing underwater acoustic signal can also enable the possibility of constellation reduction, the 8PSK and 16QAM packets are used and reduced to QPSK and 4QAM using equations 4, 6, respectively. A new random bit stream is generated. The encoding and interleaving algorithms used are the same as the original experiment. The mappings, m_n, between the new code stream c'_n and the code stream generated by constellation reduction, and p_n, between original transmitted symbols and reduced constellation symbols are obtained. The random phase and amplitude offsets are removed in the receiver right before the turbo equalization stage. In the turbo equalizer block diagram the higher order soft mapping and de-mapping are replaced by the desired lower order one and finally the estimated bit stream is decoded to compare the BER performance. Figure 14 demonstrated the improved BER performance of 8PSK and 16QAM after reducing to QPSK and 4QAM mapping scheme, respectively.
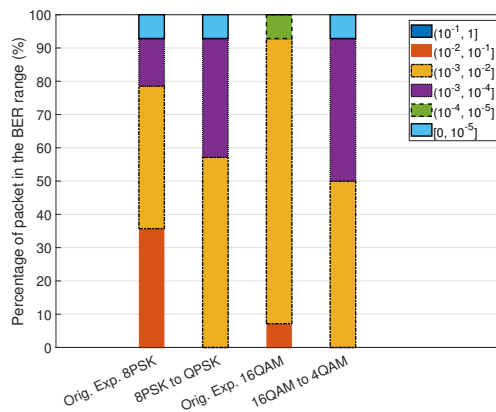

Figure 14. Packet error performance of SPACE08 experiment and reduced constellation order version of SPACE08.

5. CONCLUSIONS

In this paper we explored the possibility and proposed methods to reuse recorded signal from previously conducted underwater acoustic communication experiment in order to provide a simulator that could test newly proposed communication algorithms in real-world underwater acoustic channels. BER performance of this method is compared to the direct channel playback simulators and results show how realistically this method can simulate real-world underwater acoustic channel conditions compared to the direct playback simulators.

REFERENCES

Bjerrum-Niese, C. and Lutzen, R., 'Stochastic simulation of acoustic communication in turbulent shallow water,' IEEE Journal of Oceanic Engineering, 2000, **25**(4), pp. 523–532, ISSN 0364-9059, doi:10.1109/48.895360.

Chitre, M., 'A high-frequency warm shallow water acoustic communications channel model and measurements,' The Journal of the Acoustical Society of America, 2007, **122**, pp. 2580–6, doi:10.1121/1.2782884.

Deane, G., Preisig, J., and Singer, A. C., 'Making the most of field data to support underwater acoustic communications r&d,' in '2018 Fourth Underwater Communications and Networking Conference (UComms),' 2018 pp. 1–5, doi:10.1109/UComms.2018.8493212.

Kilfoyle, D. B. and Baggeroer, A. B., 'The state of the art in underwater acoustic telemetry,' IEEE Journal of Oceanic Engineering, 2000, **25**(1), pp. 4–27, ISSN 0364-9059, doi:10.1109/48.820733.

Peterson, J. C. and Porter, M. B., 'Ray/beam tracing for modeling the effects of ocean and platform dynamics,' IEEE Journal of Oceanic Engineering, 2013, **38**(4), pp. 655–665, ISSN 0364-9059, doi:10.1109/JOE.2013.2278914.

Porter, M. B., 'Bellhop code,' `http://oalib.hlsresearch.com/Rays/index.html`, 2019.

Qarabaqi, P. and Stojanovic, M., 'Statistical characterization and computationally efficient modeling of a class of underwater acoustic communication channels,' IEEE Journal of Oceanic Engineering, 2013, **38**(4), pp. 701–717, ISSN 0364-9059, doi:10.1109/JOE.2013.2278787.

Siderius, M. and Porter, M. B., 'Modeling broadband ocean acoustic transmissions with time-varying sea surfaces.' The Journal of the Acoustical Society of America, 2008, **124**(1).

Socheleau, F., Laot, C., and Passerieux, J., 'Parametric replay-based simulation of underwater acoustic communication channels,' IEEE Journal of Oceanic Engineering, 2015, **40**(4), pp. 796–806, ISSN 0364-9059, doi:10.1109/JOE.2015.2458211.

Song, A., Senne, J., Badiey, M., and Smith, K. B., 'Underwater acoustic communication channel simulation using parabolic equation,' in 'Proceedings of the Sixth ACM International Workshop on Underwater Networks,' WUWNet '11, ACM, New York, NY, USA, ISBN 978-1-4503-1151-9, 2011 pp. 2:1–2:5, doi:10.1145/2076569.2076571.

Stojanovic, M. and Preisig, J., 'Underwater acoustic communication channels: Propagation models and statistical characterization,' IEEE Communications Magazine, 2009, **47**(1), pp. 84–89, ISSN 0163-6804, doi:10.1109/MCOM.2009.4752682.

Tao, J., Zheng, Y. R., Xiao, C., and Yang, T. C., 'Robust mimo underwater acoustic communications using turbo block decision-feedback equalization,' IEEE Journal of Oceanic Engineering, 2010, **35**(4), pp. 948–960, ISSN 0364-9059, doi:10.1109/JOE.2010.2077831.

Tüchler, M. and Singer, A., 'Turbo equalization: An overview,' Information Theory, IEEE Transactions on, 2011, **57**, pp. 920 – 952, doi:10.1109/TIT.2010.2096033.

van Walree, P. A., Jenserud, T., and Smedsrud, M., 'A discrete-time channel simulator driven by measured scattering functions,' IEEE Journal on Selected Areas in Communications, 2008, **26**(9), pp. 1628–1637, ISSN 0733-8716, doi:10.1109/JSAC.2008.081203.

van Walree, P. A., Socheleau, F., Otnes, R., and Jenserud, T., 'The watermark benchmark for underwater acoustic modulation schemes,' IEEE Journal of Oceanic Engineering, 2017, **42**(4), pp. 1007–1018, ISSN 0364-9059, doi:10.1109/JOE.2017.2699078.

Yang, W. and Yang, T., 'High-frequency channel characterization for m-ary frequency-shift-keying underwater acoustic communications,' Acoustical Society of America Journal, 2006, **120**, pp. 2615–, doi:10.1121/1.2346133.

Yang, Z. and Zheng, Y. R., 'Iterative channel estimation and turbo equalization for multiple-input multiple-output underwater acoustic communications,' IEEE Journal of Oceanic Engineering, 2016, **41**(1), pp. 232–242, ISSN 0364-9059, doi:10.1109/JOE.2015.2398731.

Zheng, Y. R. and Xiao, C., 'Simulation models with correct statistical properties for rayleigh fading channels,' Communications, IEEE Transactions on, 2003, **51**(6), pp. 920–928.

SECTION

2. CONCLUSIONS

This dissertation proposes a new efficient and low complexity tail-biting circular MAP decoder with low computational complexity, and evaluates its performance for tail-biting convolutional codes for very short data blocks in underwater acoustic communications for both PHY and MAC layers. The performance evaluation of experimental results show that without channel equalization, FTBC codes with short packet lengths not only can perform similar to ZTC codes, in terms of BER, they can outperform the ZTC codes in terms of collision rate, and bandwidth utilization in a massive network of battery powered IoT devices, that cannot afford to use complex and power-consuming equalization algorithms. These results provide interesting suggestions that the short data blocks may suffer less from inter-symbol interference, induced by the multipath fading channels, and form packet collision; and a powerful channel code alone can be effective for communication of short data blocks over underwater acoustic channels

Second, this dissertation proposes novel methods to reuse recorded signal from previously conducted underwater acoustic communication experiment in order to provide an underwater acoustic channel simulator that could test newly proposed communication algorithms in real-world underwater acoustic channels. Packet error rate performance of the proposed method is compared to the direct channel playback simulators and results show how realistically this method can simulated real-world underwater acoustic channel conditions compared to the direct playback simulators.

3. PUBLICATIONS

1. M. Behgam, Y. R. Zheng and Z. Liu, "Tail-Biting Convolutional Codes for Underwater Acoustic Communications with Short Packets," *IEEE J. Ocean. Eng.*, Feb. 2019, [submitted]

2. M. Behgam, X. Qin, and Y. R. Zheng, "Passband Data Reuse of Field Experimental Data in Underwater Acoustic Communications," *IEEE J. Ocean. Eng.*, April. 2019, [submitted]

3. M. Behgam, Y. R. Zheng and Z. Liu, "Coding for Short Messages in Multipath Underwater Acoustic Communication Channels," *OCEANS 2018 MTS/IEEE* Charleston, Charleston, SC, 2018, pp. 1-5. doi: 10.1109/OCEANS.2018.8604711

4. S. Ebrahimi-Asl, M. Behgam, M. Zawodniok and M. T. Ghasr, "Experimental validation of minimum variance unbiased estimator of structural scattering Coefficient for an RFID antenna using linear model," *2014 IEEE International Instrumentation and Measurement Technology Conference (I2MTC) Proceedings*, Montevideo, 2014, pp. 1005-1009. doi: 10.1109/I2MTC.2014.6860894

5. M. Behgam and S. L. Grant, "Echo cancellation for bone conduction transducers," *2014 48th Asilomar Conference on Signals, Systems and Computers*, Pacific Grove, CA, 2014, pp. 1629-1632. doi: 10.1109/ACSSC.2014.7094742

REFERENCES

Anderson, J. B. and Hladik, S. M., 'Tailbiting map decoders,' IEEE Journal on Selected Areas in Communications, 1998, **16**(2), pp. 297–302.

Anderson, J. B. and Hladik, S. M., 'An optimal circular viterbi decoder for the bounded distance criterion,' IEEE Transactions on Communications, 2002, **50**(11), pp. 1736–1742.

Bahl, L., Cocke, J., Jelinek, F., and Raviv, J., 'Optimal decoding of linear codes for minimizing symbol error rate (corresp.),' IEEE Transactions on information theory, 1974, **20**(2), pp. 284–287.

Behgam, M., Zheng, Y. R., and Liu, Z., 'Coding for short messages in multipath underwater acoustic communication channels,' in 'OCEANS 2018 MTS/IEEE Charleston,' ISSN 0197-7385, 2018 pp. 1–5, doi:10.1109/OCEANS.2018.8604711.

Bjerrum-Niese, C. and Lutzen, R., 'Stochastic simulation of acoustic communication in turbulent shallow water,' IEEE Journal of Oceanic Engineering, 2000, **25**(4), pp. 523–532, ISSN 0364-9059, doi:10.1109/48.895360.

Boccardi, F., Heath, R. W., Lozano, A., Marzetta, T. L., and Popovski, P., 'Five disruptive technology directions for 5g,' IEEE Communications Magazine, 2014, **52**(2), pp. 74–80.

Chirdchoo, N., Soh, W. ., and Chua, K. C., 'Aloha-based mac protocols with collision avoidance for underwater acoustic networks,' in 'IEEE INFOCOM 2007 - 26th IEEE International Conference on Computer Communications,' ISSN 0743-166X, 2007 pp. 2271–2275, doi:10.1109/INFCOM.2007.263.

Chitre, M., 'A high-frequency warm shallow water acoustic communications channel model and measurements,' The Journal of the Acoustical Society of America, 2007, **122**, pp. 2580–6, doi:10.1121/1.2782884.

Chitre, M., Shahabudeen, S., and Stojanovic, M., 'Underwater acoustic communications and networking: Recent advances and future challenges,' Marine Technology Society Journal, 2008, **42**(1), pp. 103–116.

Clark Jr, G. C. and Cain, J. B., *Error-correction coding for digital communications*, Springer Science & Business Media, 2013.

Cox, R. V. and Sundberg, C.-E. W., 'An efficient adaptive circular viterbi algorithm for decoding generalized tailbiting convolutional codes,' IEEE transactions on vehicular technology, 1994, **43**(1), pp. 57–68.

De, S., Mandal, P., and Chakraborty, S. S., 'On the characterization of aloha in underwater wireless networks,' Mathematical and Computer Modelling, 2011, **53**(11), pp. 2093 – 2107, ISSN 0895-7177, doi:https://doi.org/10.1016/j.mcm.2010.06.041.

Deane, G., Preisig, J., and Singer, A. C., 'Making the most of field data to support underwater acoustic communications r&d,' in '2018 Fourth Underwater Communications and Networking Conference (UComms),' 2018 pp. 1–5, doi:10.1109/UComms.2018. 8493212.

Domingo, M. C., 'An overview of the internet of underwater things,' Journal of Network and Computer Applications, 2012, **35**(6), pp. 1879 – 1890, ISSN 1084-8045, doi: https://doi.org/10.1016/j.jnca.2012.07.012.

Durisi, G., Koch, T., and Popovski, P., 'Toward massive, ultrareliable, and low-latency wireless communication with short packets,' Proceedings of the IEEE, 2016, **104**(9), pp. 1711–1726.

Han, Y., Wu, T.-Y., Chen, P.-N., and Varshney, P., 'A low-complexity maximum-likelihood decoder for tail-biting convolutional codes,' IEEE Trans. Communications, 2018, **66**(5), pp. 1859 – 1870.

Heidemann, J., Stojanovic, M., and Zorzi, M., 'Underwater sensor networks: Applications, advances and challenges,' Philosophical transactions. Series A, Mathematical, physical, and engineering sciences, 2012, **370**, pp. 158–75, doi:10.1098/rsta.2011.0214.

Kilfoyle, D. B. and Baggeroer, A. B., 'The state of the art in underwater acoustic telemetry,' IEEE Journal of Oceanic Engineering, 2000, **25**(1), pp. 4–27, ISSN 0364-9059, doi:10.1109/48.820733.

Lin, S. and Costello, D. J., *Error control coding*, Pearson Education India, 2004.

Liva, G., Gaudio, L., Ninacs, T., and Jerkovits, T., 'Code design for short blocks: A survey,' arXiv preprint arXiv:1610.00873, 2016.

Ma, H. and Wolf, J., 'On tail biting convolutional codes,' IEEE Transactions on Communications, 1986, **34**(2), pp. 104–111.

Peterson, J. C. and Porter, M. B., 'Ray/beam tracing for modeling the effects of ocean and platform dynamics,' IEEE Journal of Oceanic Engineering, 2013, **38**(4), pp. 655–665, ISSN 0364-9059, doi:10.1109/JOE.2013.2278914.

Porter, M. B., 'Bellhop code,' `http://oalib.hlsresearch.com/Rays/index.html`, 2019.

Potter, J., Alves, J., Green, D., Zappa, G., McCoy, K., and Nissen, I., 'The janus underwater communications standard,' 2014 Underwater Communications and Networking, UComms 2014, 2014, doi:10.1109/UComms.2014.7017134.

Qarabaqi, P. and Stojanovic, M., 'Statistical characterization and computationally efficient modeling of a class of underwater acoustic communication channels,' IEEE Journal of Oceanic Engineering, 2013, **38**(4), pp. 701–717, ISSN 0364-9059, doi:10.1109/JOE.2013.2278787.

Raghavan, A. R. and Baum, C. W., 'A reliability output viterbi algorithm with applications to hybrid arq,' IEEE Transactions on Information Theory, 1998, **44**(3), pp. 1214–1216.

Rappaport, T. S., *Wireless Communications: Principles and Practice*, Prentice Hall PTR, 2001.

Shao, R. Y., Lin, S., and Fossorier, M. P., 'Two decoding algorithms for tailbiting codes,' IEEE transactions on communications, 2003, **51**(10), pp. 1658–1665.

Siderius, M. and Porter, M. B., 'Modeling broadband ocean acoustic transmissions with time-varying sea surfaces.' The Journal of the Acoustical Society of America, 2008, **124**(1).

Socheleau, F., Laot, C., and Passerieux, J., 'Parametric replay-based simulation of underwater acoustic communication channels,' IEEE Journal of Oceanic Engineering, 2015, **40**(4), pp. 796–806, ISSN 0364-9059, doi:10.1109/JOE.2015.2458211.

Song, A., Senne, J., Badiey, M., and Smith, K. B., 'Underwater acoustic communication channel simulation using parabolic equation,' in 'Proceedings of the Sixth ACM International Workshop on Underwater Networks,' WUWNet '11, ACM, New York, NY, USA, ISBN 978-1-4503-1151-9, 2011 pp. 2:1–2:5, doi:10.1145/2076569.2076571.

Stojanovic, M. and Preisig, J., 'Underwater acoustic communication channels: Propagation models and statistical characterization,' IEEE Communications Magazine, 2009, **47**(1), pp. 84–89, ISSN 0163-6804, doi:10.1109/MCOM.2009.4752682.

Tao, J., Zheng, Y. R., Xiao, C., and Yang, T. C., 'Robust mimo underwater acoustic communications using turbo block decision-feedback equalization,' IEEE Journal of Oceanic Engineering, 2010, **35**(4), pp. 948–960, ISSN 0364-9059, doi:10.1109/JOE.2010.2077831.

Tüchler, M. and Singer, A., 'Turbo equalization: An overview,' Information Theory, IEEE Transactions on, 2011, **57**, pp. 920 – 952, doi:10.1109/TIT.2010.2096033.

van Walree, P., Otnes, R., and Jenserud, T., 'Watermark: A realistic benchmark for underwater acoustic modems,' in '2016 IEEE Third Underwater Communications and Networking Conference (UComms),' 2016 pp. 1–4, doi:10.1109/UComms.2016.7583423.

van Walree, P. A., Jenserud, T., and Smedsrud, M., 'A discrete-time channel simulator driven by measured scattering functions,' IEEE Journal on Selected Areas in Communications, 2008, **26**(9), pp. 1628–1637, ISSN 0733-8716, doi:10.1109/JSAC.2008.081203.

van Walree, P. A., Socheleau, F., Otnes, R., and Jenserud, T., 'The watermark benchmark for underwater acoustic modulation schemes,' IEEE Journal of Oceanic Engineering, 2017, **42**(4), pp. 1007–1018, ISSN 0364-9059, doi:10.1109/JOE.2017.2699078.

Viterbi, A., 'Error bounds for convolutional codes and an asymptotically optimum decoding algorithm,' IEEE Trans. Inform. Theory, 1967, **13**(2), pp. 260 – 269.

Wang, Q. and Bhargava, V. K., 'An efficient maximum likelihood decoding algorithm for generalized tail biting convolutional codes including quasicyclic codes,' IEEE transactions on communications, 1989, **37**(8), pp. 875–879.

Williamson, A. R., Marshall, M. J., and Wesel, R. D., 'Reliability-output decoding of tail-biting convolutional codes,' IEEE Transactions on Communications, 2014, **62**(6), pp. 1768–1778.

Yang, W. and Yang, T., 'High-frequency channel characterization for m-ary frequency-shift-keying underwater acoustic communications,' Acoustical Society of America Journal, 2006, **120**, pp. 2615–, doi:10.1121/1.2346133.

Yang, Z. and Zheng, Y. R., 'Iterative channel estimation and turbo equalization for multiple-input multiple-output underwater acoustic communications,' IEEE Journal of Oceanic Engineering, 2016, **41**(1), pp. 232–242, ISSN 0364-9059, doi:10.1109/JOE.2015.2398731.

Zheng, Y. R., Wu, J., and Xiao, C., 'Turbo equalization for single-carrier underwater acoustic communications,' IEEE Communications Magazine, 2015, **53**(11), pp. 79–87, ISSN 0163-6804, doi:10.1109/MCOM.2015.7321975.

Zheng, Y. R. and Xiao, C., 'Simulation models with correct statistical properties for rayleigh fading channels,' Communications, IEEE Transactions on, 2003, **51**(6), pp. 920–928.

VITA

Mohammadhossein Behgam was born in Iran in 1988. He received the B.S. degree in electrical engineering from Azad University of Urmia, Urmia, Iran in 2010. He began his PhD study in August 2014 at the Department of Electrical and Computer Engineering at Missouri University of Science and Technology (formerly: University of Missouri-Rolla), USA. His research interests include adaptive signal processing, wireless and underwater acoustic communications. He received his Ph.D. degree in Electrical Engineering at Missouri University of Science and Technology in July 2019.